Research Paper

GEOSPHERE

GEOSPHERE; v. 12, no. 5

doi:10.1130/GES01303.1

8 figures; 6 supplemental files

CORRESPONDENCE: mpecha@email.arizona.edu

CITATION: Pecha, M.E., Gehrels, G.E., McClelland, W.C., Giesler, D., White, C., and Yokelson, I., 2016, Detrital zircon U-Pb geochronology and Hf isotope geochemistry of the Yukon-Tanana terrane, Coast Mountains, southeast Alaska: Geosphere, v. 12, no. 5, p. 1556–1574, doi:10.1130/GES01303.1.

Received 11 December 2015
Revision received 8 May 2016
Accepted 10 June 2016
Published online 22 July 2016

Detrital zircon U-Pb geochronology and Hf isotope geochemistry of the Yukon-Tanana terrane, Coast Mountains, southeast Alaska

Mark E. Pecha[1], George E. Gehrels[1], William C. McClelland[2], Dominique Giesler[1], Chelsi White[1], and Intan Yokelson[1]

[1]Department of Geosciences, University of Arizona, Tucson, Arizona 85721, USA
[2]Department of Geosciences, University of Iowa, Iowa City, Iowa 52242, USA

ABSTRACT

Rocks of the SE Alaska subterrane of the Yukon-Tanana terrane (YTTs) consist of regionally metamorphosed marine clastic strata and mafic to felsic volcanic-plutonic rocks that have been divided into the pre-Devonian Tracy Arm assemblage, Silurian–Devonian Endicott Arm assemblage, and Mississippian–Pennsylvanian Port Houghton assemblage. U-Pb geochronologic and Hf isotopic analyses were conducted on zircons separated from 23 igneous and detrital samples in an effort to reconstruct the geologic and tectonic evolution of this portion of YTT. Tracy Arm assemblage samples are dominated by Proterozoic (ca. 2.0–1.6, 1.2–0.9 Ga) and Archean (2.7–2.5 Ga) zircons that yield typical cratonal $\varepsilon_{Hf(t)}$ values. Endicott Arm assemblage samples yield U-Pb ages that range from Late Ordovician to Early Devonian and $\varepsilon_{Hf(t)}$ values that range from highly juvenile to moderately evolved. Port Houghton assemblage samples yield similar Ordovician–Devonian ages and $\varepsilon_{Hf(t)}$ values, and also include early Mississippian zircons with highly evolved $\varepsilon_{Hf(t)}$ signatures.

Comparison of these age-Hf patterns with data from nearby assemblages suggests the following: (1) Results from YTTs are similar to (or compatible with) available data from rocks of the Yukon-Tanana terrane in eastern Alaska, Yukon, and northern British Columbia (YTTn) and pericratonic strata in east-central Alaska (NAa). (2) YTTs contains abundant Late Ordovician–Early Devonian magmatism that is not recorded in YTTn and NAa. (3) The $\varepsilon_{Hf(t)}$ values from YTTs display two excursions from juvenile to evolved $\varepsilon_{Hf(t)}$ values, which are interpreted to record cycles of crustal thinning and then thickening within a convergent margin system. (4) Available data from both YTTs and YTTn support Neoproterozoic(?)–early Paleozoic positions along the northern Cordilleran margin. (5) The Late Ordovician–Early Devonian magmatic record of the southern Alexander terrane is very similar to that of YTTs, which raises the possibility that these assemblages evolved in the same convergent margin system along the northern (Alexander) and northwestern (YTT) margins of Laurentia.

These results support a tectonic model in which: (1) YTTs formed outboard of (or northward along strike of) YTTn and NAa along the northern Cordilleran margin during Neoproterozoic(?)–early Paleozoic time; (2) initial subduction-related magmatism during Late Ordovician to Early Devonian time records a progression from crustal thinning to crustal thickening, and is preserved only in YTTs; (3) a second phase of magmatism records Middle–Late Devonian crustal thinning followed by early Mississippian crustal thickening; (4) YTTs and YTTn evolved as an intra-oceanic arc outboard of the Slide Mountain ocean basin during Carboniferous–Permian time and were accreted to the continental margin during Triassic time; and (5) YTTs is interpreted to have been displaced ~1000 km southward, from an original position outboard of YTTn/NAa to its present position outboard of the Stikine terrane, along a sinistral fault system of Late Jurassic–Early Cretaceous age.

INTRODUCTION

The notion that most of the North American Cordillera is composed of suspect terranes was first introduced by Coney et al. (1980). Over the last 30+ yr, geologists have employed various geological, geophysical, and geochemical techniques in an attempt to decipher the paleogeographic history of this collage of terranes. Detrital zircon analysis has proven to be one of the most powerful tools at unraveling the complex histories of these tectonically displaced crustal fragments (e.g., Gehrels et al. 1996; Beranek at al., 2013a, 2013b; Colpron and Nelson, 2011; Gehrels, 2012, 2014). Comprehensive studies that include U-Pb ages in concert with Hf isotopic compositions provide insights into genetic relationships between juxtaposed terranes and also allow evaluation of their past interactions with cratonal sources (Malone et al., 2014; Beranek et al., 2013a, 2013b; Tochilin et al., 2014; Gehrels and Pecha, 2014). Combined U-Pb and Hf isotope analyses also reveal that terranes that are defined on the basis of geologic characteristics may consist of components with dramatically different crustal origins. An excellent example of this is provided by the Alexander terrane, which ranges from a juvenile early Paleozoic arc at the south end to a continental margin assemblage with no evidence of arc magmatism on the north end (Beranek et al., 2012, 2013a, 2013b; Tochilin et al., 2014; White et al., 2016).

This study focuses on rocks that are known or interpreted to belong to the Yukon-Tanana terrane (YTT), the main mass of which occupies a large portion of eastern Alaska, southwestern Yukon, and northwestern British Columbia (YTTn, see Fig. 1 inset). In these regions, the terrane consists of a lower assemblage of mainly siliciclastic rocks of continental margin affinity (Snowcap assemblage), a mid-Paleozoic assemblage of metasedimentary, metavolcanic, and metaplutonic rocks that formed in continental arc and back-arc settings

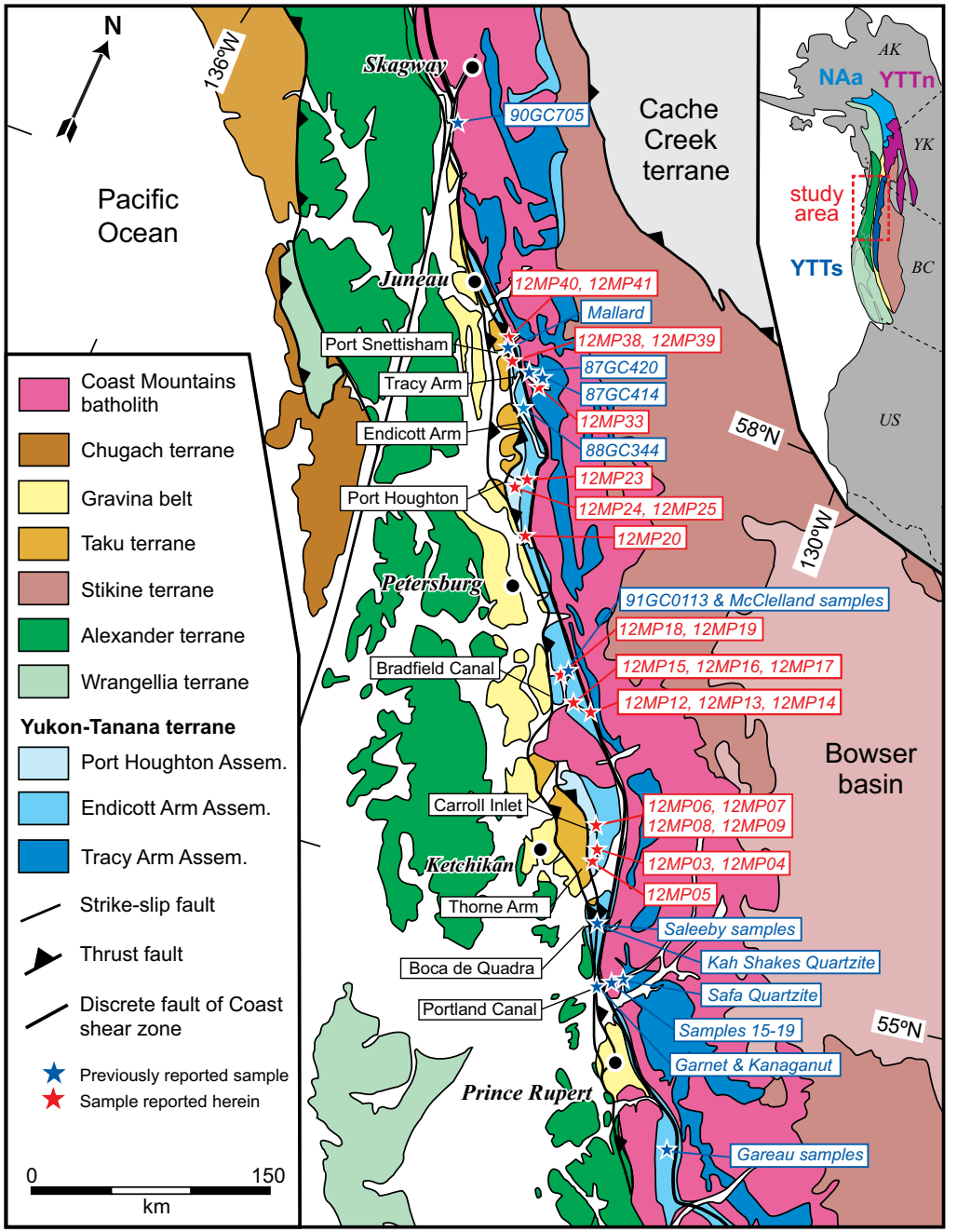

Figure 1. Generalized map showing the distribution of terranes in southeastern Alaska and along the Cordilleran margin (inset). Maps are adapted from Wheeler and McFeely (1991), Gehrels et al. (1992), Gehrels and Berg (1992), Colpron et al. (2006), and Nelson et al. (2013). Geographic names referred to in text are shown in black. Samples analyzed in this study are shown in red; samples analyzed by previous workers are shown in blue. Divisions of the Yukon-Tanana terrane (YTT) are adapted from Colpron et al. (2006) and Nelson et al. (2013) as follows: YTTs—YTT in SE Alaska; YTTn—YTT in eastern Alaska, Yukon, and northern British Columbia; NAa—pericratonic strata in east-central Alaska. AK—Alaska, YK—Yukon, BC—British Columbia, U.S.—continental United States.


DR-1 Table 1 Sample locations and descriptions
2012 SEAK DZ and IG samples

[1]Supplemental Table 1. Yukon-Tanana terrane samples and zircon images (.xls). Please visit http://dx.doi.org/10.1130/GES01303.S1 or the full-text article on www.gsapubs.org to view Supplemental Table 1.

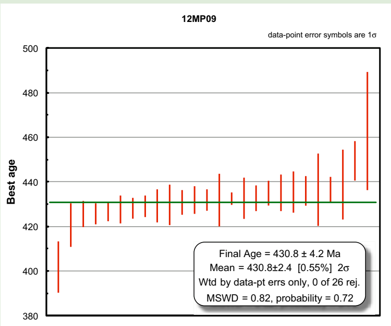

[2]Supplemental Table 2. Yukon-Tanana terrane U-Pb isotopic data (.xls). Please visit http://dx.doi.org/10.1130/GES01303.S2 or the full-text article on www.gsapubs.org to view Supplemental Table 2.

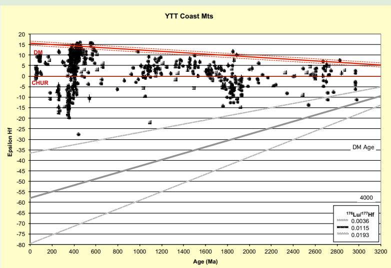

[3]Supplemental Table 3. Yukon-Tanana terrane Hf isotopic data (.xls). Please visit http://dx.doi.org/10.1130/GES01303.S3 or the full-text article on www.gsapubs.org to view Supplemental Table 3.

(Finlayson assemblage), and unconformably overlying metasedimentary and metavolcanic rocks of late Paleozoic age that accumulated in basinal and arc-type settings (Klinkit and Klondike assemblages; Mortensen, 1992; Colpron et al., 2006; Nelson et al., 2006, 2013).

Rocks that are similar to the older components of YTTn also occur to the northwest, in east-central Alaska, where they have been referred to as a pericratonic or continental margin assemblage (Dusel-Bacon et al., 2006; Colpron et al., 2006; Nelson et al., 2013). These rocks are interpreted to have remained attached to the northwestern North American margin throughout Paleozoic time, and they are referred to as NAa on Figure 1.

Rocks that are similar to the older components of YTTn also continue to the southeast, forming a narrow belt that extends southward within and west of the Coast Mountains of southeastern (SE) Alaska and northern British Columbia (Fig. 1). These rocks have been interpreted to form a southern component of YTT (Rubin et al., 1990; Rubin and Saleeby, 1991, 1992; McClelland et al., 1991, 1992; Gehrels et al., 1991, 1992; Gareau and Woodsworth, 2000; Saleeby, 2000; Gehrels, 2000, 2001; Colpron et al., 2006; Nelson et al., 2006, 2013), and they are referred to as YTTs on Figure 1. The main similarity used to support primary connections between YTTn and YTTs is the presence of pre-Devonian siliciclastic rocks of continental-margin affinity that bear abundant Precambrian detrital zircons and are overlain and intruded by mid-Paleozoic igneous rocks. Although such similarities have been noted by previous workers, the specific relationships between YTTs and YTTn remain uncertain; here, we use YTTs and YTTn to indicate that YTT may be composed of two different subterranes with somewhat different histories. The only specific connection that has been proposed for YTTs and YTTn was offered by Saleeby (2000), who used an apparent progression of Silurian–Devonian magmatism to suggest that YTTs formed outboard of YTTn.

This study utilizes U-Pb ages and Hf isotopic information from detrital zircons in metasedimentary rocks (and subordinate igneous zircons in metavolcanic and metaplutonic rocks) to characterize the main assemblages of the Yukon-Tanana terrane within and adjacent to the Coast Mountains (Supplemental Tables 1[1], 2[2], and 3[3]), reconstruct their tectonic evolution, and explore potential connections with YTTn and other assemblages in the northern Cordillera. Such comparisons are facilitated by the publication of new U-Pb/Hf data sets on detrital zircons from the Cordilleran passive margin (Gehrels and Pecha, 2014) and adjacent rocks of the Alexander terrane (Beranek et al., 2012, 2013a, 2013b; Tochilin et al., 2014; White et al., 2016), as well as the availability of detailed summaries of the geologic and tectonic evolution of YTTn and NAa (Colpron and Nelson, 2006; Colpron et al., 2006; Dusel-Bacon et al., 2006; Nelson et al., 2013). Because Hf isotope data are not yet available from zircons in YTTn or NAa, and U-Pb ages have been determined on a relatively small number of samples, we focus mainly on comparing our Hf data from YTTs with geologic and geochemical aspects of YTTn. In this comparison, we use a framework that interprets trends toward more evolved $\varepsilon_{Hf(t)}$ values to record crustal thickening, whereas trends to more juvenile $\varepsilon_{Hf(t)}$ values are the result of crustal extension or thinning (e.g., Kemp et al., 2009).

GEOLOGIC BACKGROUND OF YTTs

Rocks that are assigned to the Yukon-Tanana terrane in SE Alaska were first recognized as a distinct tectonostratigraphic assemblage, referred to as the Tracy Arm terrane, by Berg et al. (1978). These rocks were subsequently studied in detail in northern SE Alaska (Gehrels et al., 1991, 1992; Gehrels 2000), central SE Alaska (McClelland et al., 1991, 1992; McClelland and Mattinson, 2000), southern SE Alaska (Rubin and Saleeby, 1991, 1992; Saleeby, 2000), and north-coastal British Columbia (Gareau and Woodsworth, 2000; Alldrick et al., 2001; Gehrels, 2001). Three distinct assemblages were identified in most regions, including the pre-Devonian Tracy Arm assemblage, Silurian–Devonian Endicott Arm assemblage, and Mississippian–Pennsylvanian Port Houghton assemblage (Gehrels et al., 1991, 1992; McClelland et al., 1991; Gehrels, 2001). Rubin and Saleeby (1991, 1992) and Saleeby (2000) referred to similar rocks in southern SE Alaska as the pre-Devonian Kah Shakes sequence and the mid-Paleozoic to Triassic Alava sequence, and similar rocks to the south in coastal British Columbia were referred to as the Scotia-Quaal belt (Gareau and Woodsworth, 2000) or Ecstall belt (Alldrick et al., 2001).

Reconstructing the history of YTT rocks in SE Alaska is challenging due to pervasive deformation, moderate to high grades of metamorphism, and abundant plutons within and adjacent to the Coast Mountains batholith (Gehrels et al., 2009). In spite of these challenges, protolith features and relations are sufficiently preserved that researchers have been able to map the main assemblages along the length of SE Alaska and coastal British Columbia and reconstruct the main lithologic components of each assemblage. Figure 1 shows the distribution of the three components of YTTs along the length of SE Alaska and coastal British Columbia, and Figure 2 shows the reconstructed protolith relations of rocks in the three components.

Tracy Arm Assemblage

The Tracy Arm assemblage is named for a series of exposures found within Tracy Arm that form the easternmost shoreline exposures of YTTs in the Coast Mountains (Fig. 1). The rocks in this unit were included in the original Tracy Arm terrane of Berg et al. (1978) and Monger and Berg (1987). Dominant rock types are biotite schist, gneiss, quartzite, and marble, with the majority being metamorphosed to amphibolite facies. Metamorphism of these rocks is due at least in part to the proximity of mid-Cretaceous to Early Tertiary plutons of the Coast Mountains batholith (Stowell and Crawford, 2000; Gehrels et al., 2009). Rocks of the Tracy Arm assemblage are highly deformed, with a strong foliation and common isoclinal folds (Fig. 3A). These rocks are interpreted to be mainly Neoproterozoic–early Paleozoic in age because they contain abundant Mesoproterozoic and older detrital zircons (Gehrels et al., 1991, 1992; Saleeby, 2000; Gehrels, 2000, 2001) and are intruded by plutons of Silurian and Devonian age. They are interpreted to have formed in a shelf environment along a passive continental margin, given the widespread occurrence of metaclastic quartzite (Fig. 3B) and marble, along with the abundance of Precambrian detrital zircons.

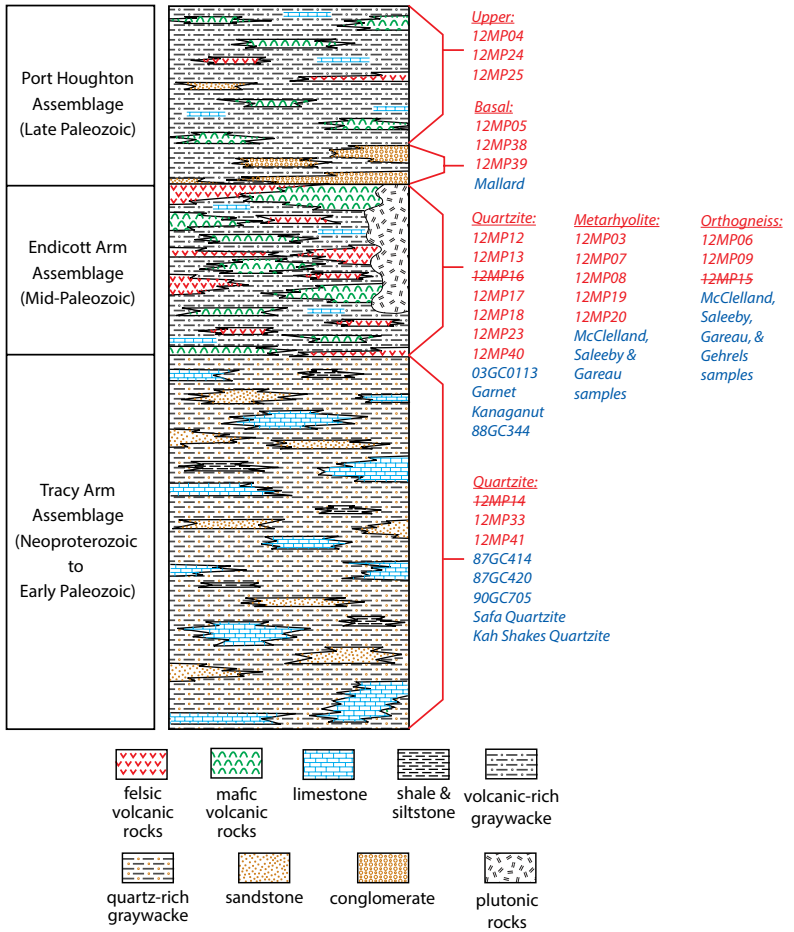

Figure 2. Schematic stratigraphic section of the Yukon-Tanana terrane in the Coast Mountains of SE Alaska (adapted from Gehrels et al., 1992). Approximate positions of samples are shown. Sample numbers in red are from this study, with strikethrough indicating that analyses are compromised by metamorphism. Samples in blue are from previous studies (McClelland et al., 1991; Gehrels et al., 1991; Gehrels and Kapp, 1998; McClelland and Mattinson, 2000; Gareau and Woodsworth, 2000; Saleeby, 2000; Gehrels, 2000, 2001).

Endicott Arm Assemblage

The Endicott Arm assemblage represents a magmatic arc assemblage named for a series of shoreline exposures along Endicott Arm (Fig. 1). The succession gradationally overlies the Tracy Arm assemblage and consists mainly of mafic, intermediate, and felsic metavolcanic rocks (Fig. 3C), interbedded with volcanic-rich metasediments (graywacke) and subordinate marble (limestone; Gehrels et al., 1992) and intruded by mainly felsic to intermediate-composition metaplutonic bodies (Fig. 3D). Previous geochronologic analyses of both felsic metavolcanic and metaplutonic rocks of the Endicott Arm assemblage yielded Silurian and Devonian ages ranging from ca. 440 to ca. 360 Ma (McClelland et al., 1991; Gehrels et al., 1992; Saleeby, 2000; Gareau and Woodsworth, 2000; McClelland and Mattinson, 2000; Alldrick et al., 2001; Gehrels, 2001).

Port Houghton Assemblage

The Port Houghton assemblage is characterized by quartz-rich metaclastic rocks (commonly fine-grained turbidites; Fig. 3E), interbedded locally with mafic to felsic volcanic rocks and subordinate marble (Gehrels et al., 1992). It also contains a distinctive basal metaconglomerate (Fig. 3F) that bears clasts of metagraywacke, quartzite, metarhyolite, and metaplutonic clasts of intermediate to felsic composition. The Port Houghton assemblage rests unconformably on the Endicott Arm assemblage (Gehrels et al., 1992; Gehrels and Kapp, 1998).

GEOLOGIC BACKGROUND OF YTTn AND NAa

Within eastern Alaska, Yukon, and northern British Columbia, YTTn has been described as a regionally metamorphosed pre-Triassic assemblage that includes Neoproterozoic(?)–Paleozoic metasedimentary and metavolcanic rocks that are intruded by Late Devonian to Late Permian plutons (Templeman-Kluit, 1976, 1979; Coney et al., 1980; Hansen, 1990; Mortensen, 1992; Piercey et al., 2004, 2006; Dusel-Bacon et al., 2004, 2006, 2013; Colpron et al., 2006; Murphy et al., 2006; Nelson et al., 2006, 2013). The basal units of YTTn are primarily metamorphosed quartzite, pelite, and marble, referred to as the Snowcap assemblage, that are interpreted to have formed in a passive continental margin setting (Colpron et al., 2006; Piercey and Colpron, 2009). Workers in the region have interpreted that during Late Devonian time, the passive-margin environment evolved into a convergent margin system, with widespread magmatism during Late Devonian through early Mississippian time (Finlayson assemblage), followed by accumulation of conglomeratic strata and overlying volcanic rocks and clastic strata of middle Mississippian through Early Permian age (Klinkit assemblage; Colpron et al., 2006; Nelson et al., 2013).

Farther north and west from YTTn, underlying a large region of east-central Alaska and western Yukon, there are metasedimentary, metavolcanic, and metaplutonic rocks of mainly early to mid-Paleozoic age that are referred to as North American pericratonic rocks (Dusel-Bacon et al., 2006; NAa in the inset of Fig. 1). Although most workers agree that YTTn and NAa share a similar early and mid-Paleozoic history, YTTn and NAa are grouped as separate tectonic entities because they were apparently separated during late Paleozoic time by the broad Slide Mountain ocean basin (Dusel-Bacon et al., 2004, 2006, 2013; Colpron et al., 2006; Nelson et al., 2006, 2013).

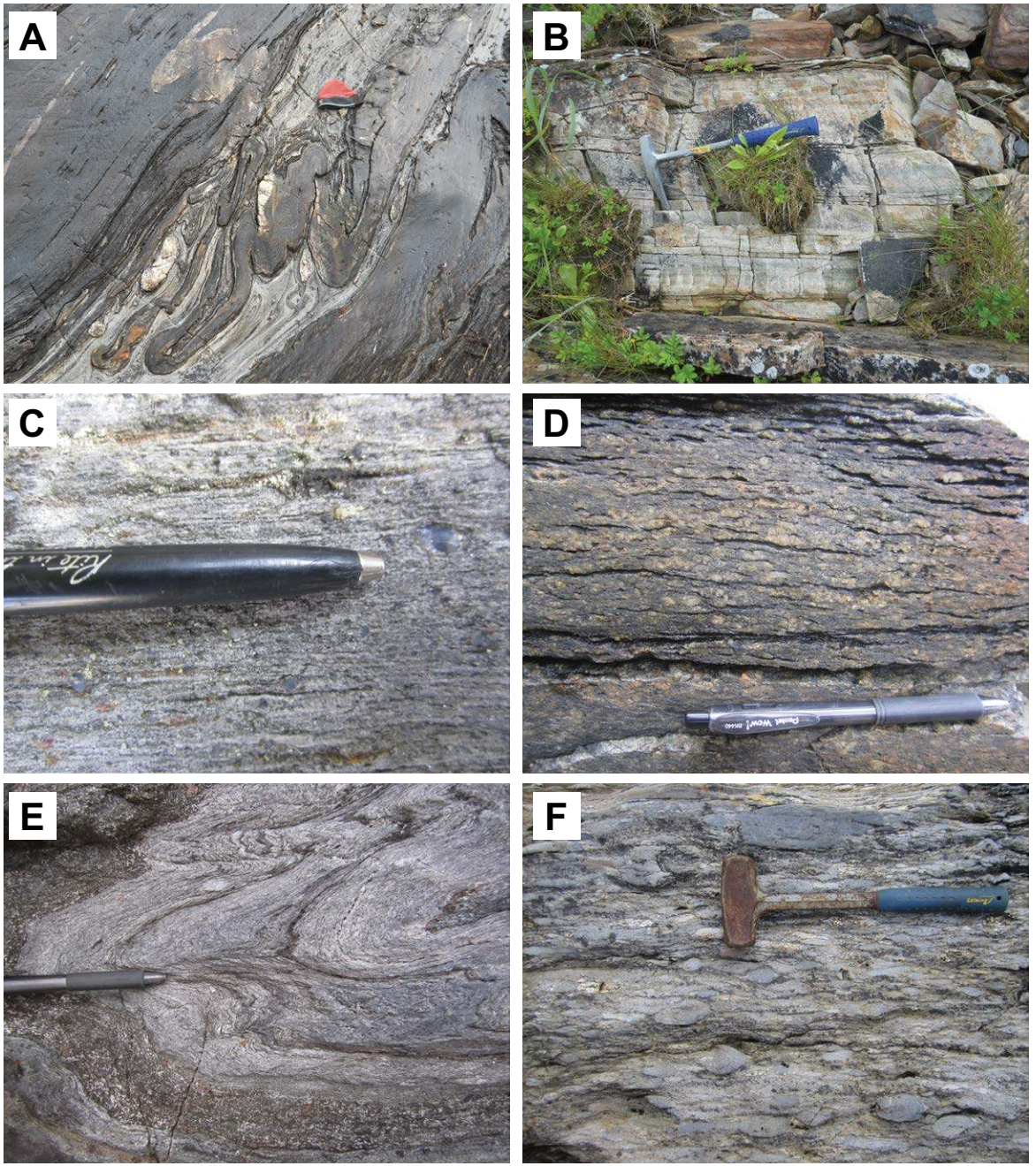

Figure 3. Representative outcrop photographs of samples analyzed in this study: (A) folded quartzite and marble of the Tracy Arm assemblage (sample 12MP33); (B) metaclastic quartzite of the Tracy Arm assemblage (sample 12MP41); (C) quartz-porphyritic metarhyolite of the Endicott Arm assemblage (sample 12MP19); (D) coarse-grained metatrondhjemite of the Endicott Arm assemblage (sample 12MP09) with mid-Cretaceous mylonitic fabric; (E) highly folded quartz-rich metaturbidite of the upper Port Houghton assemblage (sample 12MP25); (F) pebble to cobble metaconglomerate of the basal Port Houghton assemblage (sample 12MP38).

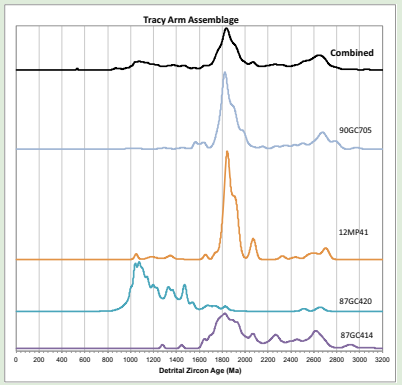

[4]Supplemental Table 4. Tracy Arm probability plots (.xls). Please visit http://dx.doi.org/10.1130/GES01303.S4 or the full-text article on www.gsapubs.org to view Supplemental Table 4.

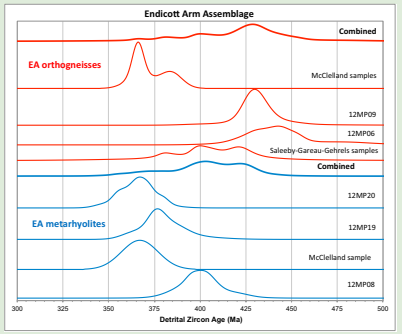

[5]Supplemental Table 5. Endicott Arm probability plots (.xls). Please visit http://dx.doi.org/10.1130/GES01303.S5 or the full-text article on www.gsapubs.org to view Supplemental Table 5.

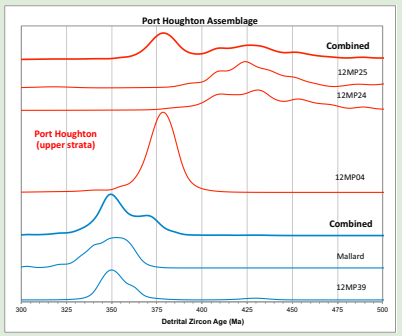

[6]Supplemental Table 6. Port Houghton probability plots (.xls). Please visit http://dx.doi.org/10.1130/GES01303.S6 or the full-text article on www.gsapubs.org to view Supplemental Table 6.

The magmatic evolution of YTTn and NAa is recorded in six cycles of Paleozoic igneous activity (Colpron et al., 2006; Nelson et al., 2006, Piercey et al., 2006), giving YTTn and NAa a distinct magmatic and geochronologic fingerprint. The six cycles, as described by Nelson et al. (2006), are as follows.

(1) Pre–cycle I (older than 395 Ma): Pre–cycle I is characterized by accumulation of Proterozoic(?)–Lower Paleozoic passive-margin strata along the rifted margin of northwestern Laurentia. These rocks are interpreted to be the oldest components in YTTn and NAa.

(2) Cycle I (Middle to Late Devonian; 395–365 Ma): Magmatism of this cycle occurred mainly within YTTs; however, it includes the onset of extensional (back-arc?) magmatism in NAa at ca. 375 Ma and in YTTn at ca. 365 Ma.

(3) Cycle II (Late Devonian–early Mississippian; 365–357 Ma): This cycle records significant magmatism in both YTTn and NAa, with compositions that are commonly bimodal. Felsic magmas are mainly of crustal derivation. Regional extension occurred within this broad arc/back-arc system and is also recorded by mid-Paleozoic extensional faults, volcanic rocks, and sedimentary exhalative and volcanogenic massive sulfide base-metal deposits within adjacent passive-margin strata.

(4) Cycle III (early Mississippian; 357–342 Ma): This cycle is characterized by widespread arc-type magmatism (especially in YTTn) accompanied by deformation and accumulation of conglomeratic strata. Eastern YTTn experienced back-arc/extensional magmatism that marks the onset of rifting of the YTTn pericratonic arc from the North American continental margin, forming the Slide Mountain ocean basin. NAa experienced waning magmatism during this period and is interpreted to have remained attached to the continental margin.

(5) Cycle IV (late Mississippian; 342–314 Ma): This cycle is marked by a regional deformational event, erosion of Late Devonian–early Mississippian arc assemblages, widespread accumulation of conglomeratic strata, and a shift to more primitive, andesitic volcanism within YTTn.

(6) Cycle V (Pennsylvanian–Early Permian; 314–269 Ma): This cycle records mafic to intermediate-composition volcanism within an extensional arc setting.

(7) Cycle VI (Middle and Late Permian; 269–253 Ma): This cycle is marked by magmatism and deformation along the inboard margin of YTTn due to subduction of the Slide Mountain ocean basin. Closure of the ocean basin, accretion of YTTn, and cessation of magmatism all occurred by Middle Triassic time.

PREVIOUSLY PUBLISHED U-Pb GEOCHRONOLOGIC DATA FROM YTTs

U-Pb geochronologic studies of detrital zircons from each of the three assemblages in YTTs have been conducted previously. Results are summarized here, and all ages are compiled and plotted in Supplemental Tables 2, 4[4], 5[5], and 6[6]. No Hf analyses have been reported previously.

Quartzites from the Tracy Arm assemblage have been analyzed from the length of SE Alaska (Gehrels et al., 1991; Gehrels, 2000, 2001). From south to north: (1) 110 U-Pb ages have been obtained on quartzite from Portland Canal (Safa Islands), with dominant age groups of 2810–2420, 2080–1730, 1520–1330, and 1260–810 Ma; (2) 100 ages have been obtained on quartzite from near Boca de Quadra (Kah Shakes), with dominant ages of 2740–2460, 2410–2040, 1960–1670, and 1460–1090 Ma; (3) 229 ages have been obtained from two quartzites in Tracy Arm (87GC414 and 87GC420), with dominant age groups of 2720–2510 and 2110–1620 Ma in one sample and 1490–1300 and 1250–950 Ma in a second sample; and (4) 131 ages have been obtained on quartzite from north of Juneau (90GC705), with dominant age groups of 2820–2570 and 2020–1730 Ma.

Quartzite, metarhyolite, and metaplutonic rocks of the Endicott Arm assemblage have also been analyzed from various regions of SE Alaska and coastal British Columbia. Four quartzite samples have been studied near Boca de Quadra and Endicott Arm, with dominant age groups of 417–310 Ma and subordinate age groups of 2000–1520, 1500–1360, 1320–990, and 505–450 Ma (Gehrels, 2001). Metarhyolites have also been analyzed, with ages of ca. 370 Ma from near Prince Rupert (Gareau and Woodsworth, 2000), 422–412 Ma from near Boca de Quadra Canal (Saleeby, 2000), and 384–366 Ma near Petersburg (McClelland et al., 1991; McClelland and Mattinson, 2000). Orthogneisses that are associated with rocks of the Endicott Arm and Tracy Arm assemblages have yielded ages of ca. 385 Ma near Prince Rupert (Gareau and Woodsworth, 2000), 429–380 Ma near Portland Canal (Gehrels, 2001), 424–383 Ma from near Boca de Quadra (Saleeby, 2000), and 367–345 Ma near Petersburg (McClelland et al., 1991; McClelland and Mattinson, 2000).

Metaconglomerate of the Port Houghton assemblage has been analyzed previously from Port Snettisham (Gehrels and Kapp, 1998). U-Pb ages have been reported for 154 detrital zircon grains, with dominant age groups of 2010–1760 and 370–310 Ma, and a small number of 2710–2560 Ma ages.

ANALYTICAL METHODS

We collected ~15 kg of homogeneous rock for each detrital zircon sample. Zircon grains were extracted using traditional methods of jaw crushing and pulverizing, followed by density separation using a Wilfley table and heavy liquids. The resulting heavy mineral fraction then underwent further separation using a Frantz LB-1 magnetic barrier separator. A representative split of the zircon yield was incorporated into a 1 in. (2.5 cm) epoxy mount along with multiple fragments of the primary U-Pb Sri Lanka (SL) zircon standard, and the Hf standards R33, Mud Tank, FC-1, Plesovice, Temora, and 91500. The mounts were sanded down to ~20 μm, polished to 1 μm, and imaged by backscattered electron (BSE) cathodoluminescence (CL) imaging using a Hitachi S-3400N scanning electron microscope (SEM; www.geoarizonasem.org). Prior to isotopic analysis, mounts were cleaned in an ultrasonic bath of 1% HNO_3 and 1% HCl in order to remove surficial common Pb.

U-Pb Geochronologic Analysis

U-Pb geochronology of individual zircon crystals was conducted by laser ablation–multicollector–inductively coupled plasma–mass spectrometry (LA-MC-ICP-MS) at the Arizona LaserChron Center (Gehrels et al., 2008; Gehrels

and Pecha, 2014; www.laserchron.org). The isotopic analyses involved ablation of zircon using a Photon Machines Analyte G2 excimer laser (λ = 193 nm) coupled to a Nu Instruments high-resolution (HR) MC-ICP-MS. Ultrapure helium carried the ablated material into the plasma source of the ICP-MS, which was equipped with a flight tube of sufficient width that U, Th, and Pb isotopes could be measured simultaneously. Depending on the size of the zircons, analyses were conducted utilizing either Faraday collectors or ion counters for measurement of ^{208}Pb, ^{207}Pb, and ^{206}Pb (see Supplemental Table 2 for specific U-Pb methods used on each sample).

The majority of the U-Pb analyses were conducted with a 30 μm spot diameter using a Faraday acquisition routine consisting of one 15 s integration on peaks with the laser off (for backgrounds), fifteen 1 s integrations with the laser firing, and a 30 s delay to ensure that the previous sample was completely purged from the system. Faraday detectors with 3 × 10^{11} ohm resistors measured ^{238}U, ^{232}Th, and ^{208}Pb, ^{207}Pb, and ^{206}Pb, and discrete dynode ion counters measured ^{204}Pb and ^{202}Hg, all in static mode. Drill rate was ~1 μm/s, resulting in a final ablation pit depth of ~15 μm.

An ion counter routine was employed for samples with zircons that were too small to accommodate a 30 μm spot. These analyses utilized a 20 μm beam diameter and consisted of one 12 s integration on peaks with the laser off (for backgrounds), twelve 1 s integrations with the laser firing, and a 30 s delay to purge the previous sample. During this routine, Faraday detectors measured ^{238}U and ^{232}Th, and discrete dynode ion counters measured ^{208}Pb, ^{207}Pb, ^{206}Pb, and ^{204}Pb, also in static mode. Drill rate was ~1 μm/s, resulting in a final ablation pit depth of ~12 μm.

Approximately 105 analyses were conducted on each sample with one U-Pb measurement per grain. Grains were selected in random fashion, with crystals rejected only on the basis of small size or the presence of cracks or inclusions. The use of high-resolution BSE images for detrital samples and detailed cathodoluminescence (CL) images for igneous samples provided assistance in grain selection and spot placement (see Supplemental Table 1 for CL images of representative zircons from each sample).

Data reduction was accomplished using NUPMagecalc.xls, which is a standard Arizona LaserChron Center reduction protocol (Gehrels et al., 2008; Gehrels and Pecha, 2014). The specific filters (e.g., discordance, $^{206}Pb/^{238}U$ precision, $^{206}Pb/^{207}Pb$ precision, etc.) used during the data treatment are indicated in the notes in Supplemental Table 2. Data are presented on normalized age-probability diagrams, which sum all relevant analyses and uncertainties and then divide by the number of analyses such that each curve contains the same area (e.g., Fig. 4). Age groups are characterized by the ages of their peaks in age probability and by the range of constituent ages.

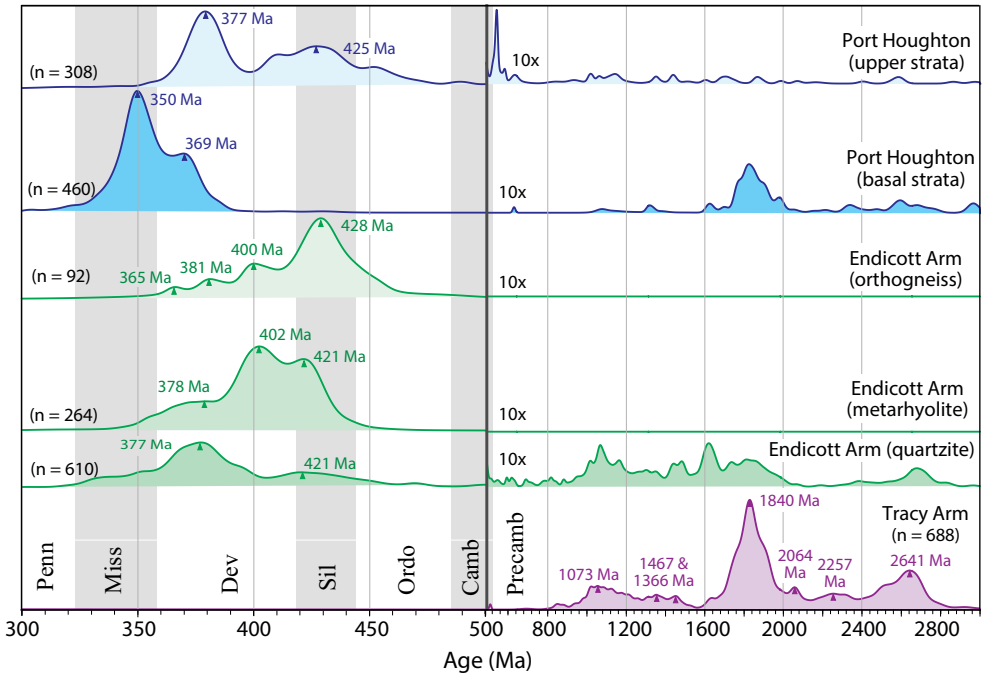

Figure 4. U-Pb geochronologic results for YTTs. Each curve is the sum of ages and uncertainties from all analyses of a set of samples (from Figure 2). The area under each curve is normalized according to the number of constituent analyses (Gehrels, 2012, 2014). Peaks in age probability are shown for each set of samples (from Supplemental Table 2). Ages for individual samples are shown on stacked age-distribution diagrams presented in Supplemental Tables 4 (Tracy Arm), 5 (Endicott Arm), and 6 (Port Houghton). Time scale is from Cohen et al. (2013). Penn—Pennsylvanian; Miss—Mississippian; Dev—Devonian; Sil—Silurian; Ordo—Ordovician; Camb—Cambrian; Precamb—Precambrian.

Hf Isotopic Analysis

Hf isotope geochemistry of zircons was conducted by LA-MC-ICP-MS at the Arizona LaserChron Center following established analytical protocols reported in Cecil et al. (2011) and Gehrels and Pecha (2014). Approximately 50 Hf analyses were conducted per detrital sample, with grains selected to represent each main age group, and to avoid crystals with discordant or imprecise ages. CL images (examples for each sample are located in Supplemental Table 1) were utilized for navigation/spot location, ensuring that all Hf analyses were within the same growth zone/domain as the U-Pb pit. In most cases, Hf laser pits were located directly on top of the U-Pb analysis pits. Complete Hf isotopic data, including Hf-evolution plots of individual samples, are presented in Supplemental Table 3.

Hf data are presented using Hf evolution diagrams (Fig. 5), where initial $^{176}Hf/^{177}Hf$ ratios are expressed in $\varepsilon_{Hf(t)}$ notation, which represents the Hf isotopic composition at the time of zircon crystallization relative to the chondritic uniform reservoir (CHUR; Bouvier et al., 2008). Internal precision for $^{176}Hf/^{177}Hf$ and $\varepsilon_{Hf(t)}$ is reported for each analysis on Hf evolution plots in Supplemental Table 3, and as the average for all analyses (2.4 epsilon units at 2σ) on Figure 5. Based on the in-run analysis of zircon standards, the external precision is 2–2.5 epsilon units (2σ). The Hf isotopic evolution of typical felsic crust is shown with arrows on the ε_{Hf} evolution diagrams, based on a $^{176}Lu/^{177}Hf$ ratio of 0.0115 (Vervoort and Patchett, 1996; Vervoort et al., 1999).

U-Pb AGES AND Hf ISOTOPIC RESULTS

In total, 25 samples were collected from YTTs with the intent of obtaining both U-Pb geochronologic and Hf isotopic data (Supplemental Table 1). Locations of the 23 samples that yielded zircons are shown on Figure 1, and their stratigraphic assignments are shown on Figure 2. Final U-Pb and Hf results for all samples are reported in Supplemental Tables 2 and 3. To assist with interpretation, samples are discussed according to their stratigraphic assignment (Tracy Arm assemblage, Endicott Arm assemblage, or Port Houghton assemblage). Summary plots of the ages available from each assemblage are shown on Figure 4, and stacked age-distribution diagrams for individual samples are presented in Supplemental Table 4 (Tracy Arm), Supplemental Table 5 (Endicott Arm), and Supplemental Table 6 (Port Houghton).

Complications in U-Pb Systematics

Proximity of the YTTs to Jurassic through Early Tertiary plutons of the Coast Mountains batholith (McClelland and Mattinson, 2000; Stowell and Crawford, 2000) has resulted in the occurrence of ages in several samples that are younger than the protolith depositional age. In most cases, these ages overlap with ages of nearby plutonic bodies and are interpreted to record metamorphic zircon growth given their elevated U/Th (Rubatto, 2002) and/or occurrence of metamorphic textures observed in BSE or CL images. In some cases, zircon grains yielded similar Mesozoic ages but had typical igneous values for U/Th and typical oscillatory zoning in BSE or CL images. These grains may also be metamorphic in origin, or it is possible that they are from small veins or leucosomes containing Mesozoic zircon that were not recognized during sample collection. A third mode of complexity is the occurrence in some samples of zircon grains that are younger than the known depositional age but older than the ages of nearby plutons. In most cases, these ages are characterized by higher than average U concentration, and they are interpreted to have experienced partial Pb loss. Analyses that are compromised by any of the complexities noted here are highlighted in Supplemental Table 2 and are not considered further here.

Results from Tracy Arm Assemblage

Sample 12MP33 is a quartzite interlayered with marble that is exposed in eastern Tracy Arm (Fig. 3A). The U-Pb age distribution is dominated by Paleoproterozoic ages of 2491–1736 Ma (peaks at 1828 and 1770 Ma), with subordinate Archean zircons ranging from 2677 to 2521 Ma (peak at 2668 Ma). The $\varepsilon_{Hf(t)}$ ratios of the Paleoproterozoic zircons range from +4 to –13, and the Archean grains are exclusively juvenile, ranging from +7 to +2 (Fig. 5).

A quartzite (12MP41) collected in Port Snettisham (Fig. 3B) produced similar Paleoproterozoic ages, ranging from 2440 to 1737 Ma (peaks at 2083, 1912, and 1847 Ma), along with subordinate Archean ages ranging from 2719 to 2543 Ma (peak at 2713 Ma). The Archean zircons are predominantly juvenile (+7 to +2 $\varepsilon_{Hf(t)}$), whereas the Paleoproterozoic grains display more evolved $\varepsilon_{Hf(t)}$ values clustering between +3 and –15.

Collectively, the two new samples combined with previously published results from the Tracy Arm assemblage yield an age distribution with a dominant age group of 1970–1710 Ma (age peak at 1840 Ma), and subordinate age groups of 2350–2170 Ma (peak at 2257 Ma), 2750–2460 Ma (peak at 2641 Ma), 2100–2035 Ma (peak at 2064 Ma), 1490–1320 Ma (peaks at 1467 and 1366 Ma), and 1250–970 (peak at 1073 Ma; Fig. 4). Hf results for the Tracy Arm assemblage are generally juvenile for Archean grains and evolved to intermediate composition for Paleoproterozoic grains (Supplemental Table 3; Fig. 5).

Results from Endicott Arm Assemblage Metavolcanic Rocks

Metavolcanic rocks of the Endicott Arm assemblage have been analyzed from several different localities in SE Alaska (Fig. 1). From south to north, these include (1) a quartz-porphyritic metarhyolite from Thorne Arm (12MP03) that yielded a weighted mean age of 403.0 ± 3.4 Ma, (2) two metarhyolite samples in Carroll Inlet (12MP07 and 12MP08) that yielded weighted mean ages of 423.6 ± 4.8 Ma and 401.1 ± 4.5 Ma (respectively), (3) a metarhyolite (Fig. 3C) from near Bradfield Canal (12MP19) that yielded a weighted mean age of 377.3 ± 4.8 Ma, and (4) a metarhyolite from near Petersburg (12MP20) that yielded a weighted mean age of 368.9 ± 5.1 Ma (same sample for which

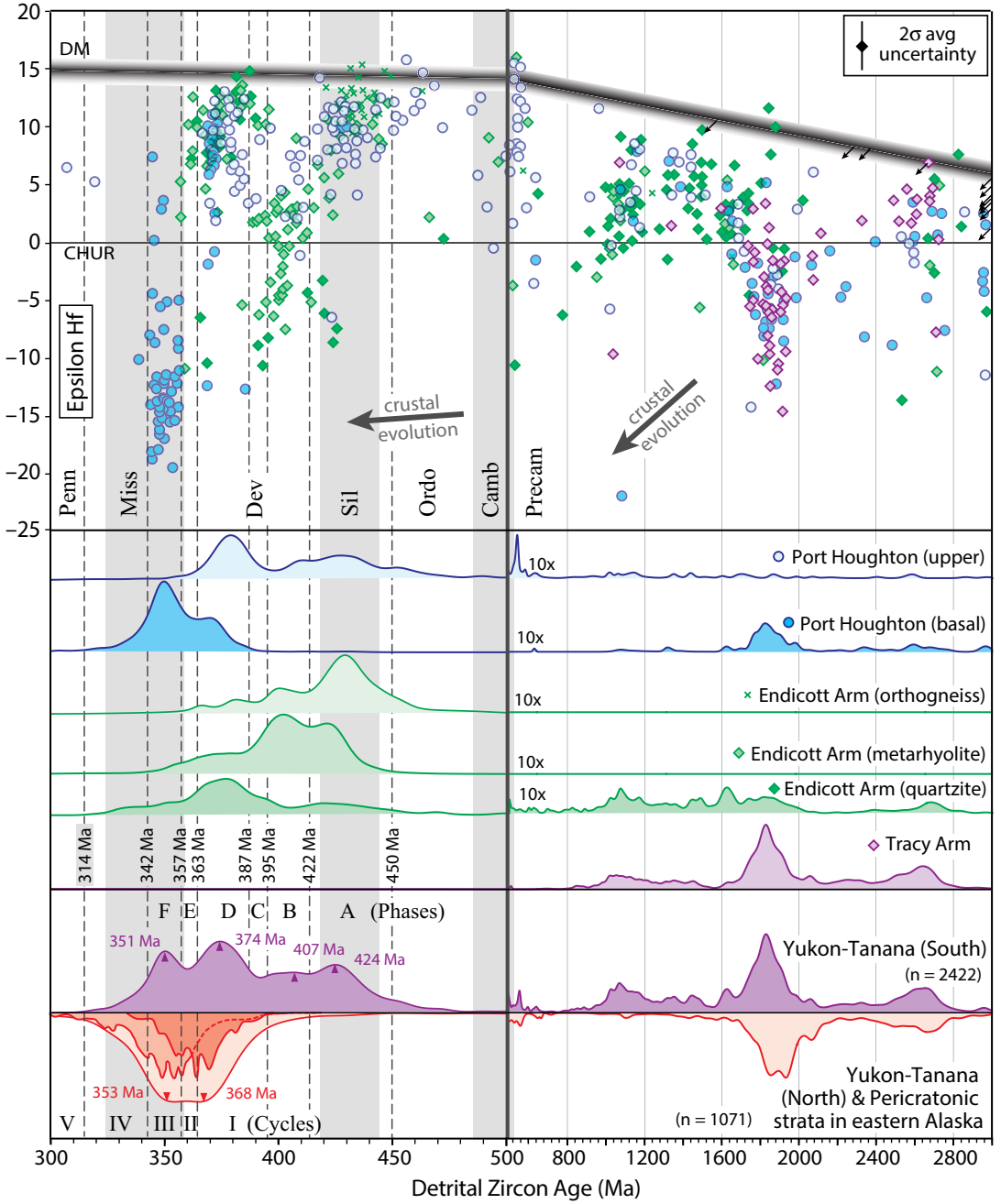

Figure 5. Hf isotopic data for YTTs (upper panel), and comparison of U-Pb ages for YTTs and YTTn/NAa (lower panel). Note break in age at 500 Ma, and 10× vertical exaggeration of pre–500 Ma grains of some age distributions. Age-distribution diagrams for individual components of YTTs are from Figure 4. Lower age-distribution curve for YTTs is the sum of all ages presented from rocks in SE Alaska. Age-distribution curves for YTTn/NAa include all available U-Pb detrital zircon ages from YTTn (light red curve; from compilation in Supplemental Table 2), and curves for all igneous ages from YTTn (medium shading) and NAa (darker shading; from fig. 4 *of* Nelson et al., 2006). Note that dashed portion of the YTTn curve is an overestimate because it includes several ages older than 360 Ma from YTTs. Vertical dashed lines are the time divisions separating the phases described herein and the cycles reported in Figure 4 of Nelson et al. (2006). In upper panel, Hf isotopic analyses are separated according to rock type and assemblage. Average uncertainty of all analyses is 2.4 epsilon units (at 2σ). Average crustal evolution is based on $^{176}Lu/^{177}Hf$ ratio of 0.0115 (Vervoort and Patchett, 1996; Vervoort et al., 1999; Amelin et al., 1999, 2000). Small arrows in upper panel represent Hf evolution lines for whole-rock Hf isotope data from metasedimentary rocks of the Snowcap Assemblage of YTTn (Piercey and Colpron, 2009). DM—depleted mantle; CHUR—chondritic uniform reservoir; Penn—Pennsylvanian; Miss—Mississippian; Dev—Devonian; Sil—Silurian; Ordo—Ordovician; Camb—Cambrian; Precamb—Precambrian.

McClelland et al. [1991] reported an isotope dilution–thermal ionization mass spectrometry age of 367 ± 10 Ma; all uncertainties at 2σ; data and plots presented in Supplemental Table 2). Collectively, these five ages combined with the previously published analyses of Endicott Arm assemblage metavolcanic rocks yield a bimodal distribution of ages between 425 and 355 Ma, with age peaks at 421, 402, and 378 Ma (Fig. 4). The $\varepsilon_{Hf(t)}$ values for the metarhyolites are also bimodal, with intermediate (+5 to –8) values for ca. 420–390 Ma analyses and mostly juvenile values (+12 to +2) for 390–355 Ma analyses (Supplemental Table 3; Fig. 5).

Results from Endicott Arm Assemblage Metaplutonic Rocks

Metaplutonic rocks were analyzed from two samples collected from Carroll Inlet (Fig. 1). The resulting ages are 438.5 ± 5.0 Ma (sample 12MP06) and 430.8 ± 4.2 Ma (sample 12MP09; Fig. 3D; all weighted mean uncertainties reported at 2σ; data and plots presented in Supplemental Table 2). When combined with analyses of metarhyolite from other areas of YTTs, the resulting age distribution has peaks in age probability of 428, 400, 381, and 365 Ma (Fig. 4). The $\varepsilon_{Hf(t)}$ values for the metaplutonic rocks are juvenile (+15 to +9) for Silurian samples, and no data are available for Devonian samples (Supplemental Table 3; Fig. 5).

Results from Endicott Arm Assemblage Metasedimentary Rocks

Six samples collected from Endicott Arm assemblage metasedimentary rocks provided reliable U-Pb data. All samples yielded a mix of Precambrian and early Paleozoic ages, with variable proportions of the two age groups (Supplemental Tables 2 and 5). With data from previously reported analyses and all six of our samples combined, the age distribution of early Paleozoic grains is bimodal, with ages ranging from ca. 450 to ca. 350 Ma and age peaks of 421 and 377 Ma (Fig. 4). Precambrian grains are present in several distinct age groups of 2770–2620 Ma (peak age of 2694 Ma), 1890–1580 Ma (peak ages of 1732 and 1620 Ma), 1520–1415 Ma (peak ages of 1485 and 1444 Ma), and 1200–930 Ma (peak ages of 1168, 1077, and 1026 Ma; Fig. 4). The $\varepsilon_{Hf(t)}$ values for Paleozoic grains are variable, with two samples (12MP23 and 12MP40) yielding mainly juvenile values and three samples (12MP12, 12MP13, and 12MP18) yielding more-evolved values (Supplemental Table 3; Fig. 5). The $\varepsilon_{Hf(t)}$ values for Precambrian grains are quite similar to those from the Tracy Arm assemblage (Fig. 5).

Results from Port Houghton Assemblage Metasedimentary Rocks

The U-Pb and Hf data for detrital zircons from basal conglomerates of the Port Houghton assemblage and from overlying strata are different. Results from these two units are accordingly described separately.

U-Pb ages from the basal conglomeratic strata are similar in all three samples (12MP05, 12MP38, and 12MP39; Fig. 3F), with predominantly early Paleozoic ages and subordinate Precambrian ages. When previously reported analyses and data from our three samples are combined, ages range from ca. 390 to ca. 325 Ma, with age peaks of 369 and 350 Ma (Supplemental Tables 2 and 6; Fig. 4). Precambrian grains yield one main age group, extending from 2030 to 1730 Ma, with age peaks at 2001 and 1831Ma. The $\varepsilon_{Hf(t)}$ values for the early Paleozoic grains are mostly juvenile to intermediate (+11 to –2) for ca. 369 Ma grains and more evolved (+7 to –20) for slightly younger grains (Supplemental Table 3; Fig. 5). The Precambrian grains yield $\varepsilon_{Hf(t)}$ values that are similar to those for the Tracy Arm assemblage and Endicott Arm assemblage (Fig. 5).

U-Pb ages from overlying sandstones (12MP04, 12MP24, and 12MP25; Fig. 3E) are different from ages in the conglomeratic strata, with early Paleozoic grains that are somewhat older and Precambrian ages that are variable (Supplemental Table 2; Fig. 4). The younger grains yield a bimodal distribution ranging from ca. 455 to ca. 345 Ma, with age peaks at 425 and 377 Ma (Fig. 4). The Precambrian grains range from Archean to Neoproterozoic, with numerous grains ranging from 670 to 530 Ma (Fig. 4). The $\varepsilon_{Hf(t)}$ values are juvenile to intermediate (mostly between +13 to +2) for all early Paleozoic grains, mostly juvenile (+15 to +7) for Neoproterozoic grains, and similar to the Tracy Arm and Endicott Arm assemblages for Precambrian grains (Supplemental Table 3; Fig. 5).

DISCUSSION

YTTs Magmatic History

The U-Pb geochronologic and Hf isotopic data presented herein provide a detailed record of Ordovician though Carboniferous magmatism in YTTs. The composite of this record is shown on Figure 5, with a single age-probability curve that includes results from all metasedimentary, metavolcanic, and metaplutonic samples ($n = 2422$). Peaks in age probability occur at 424, 407, 374, and 351 Ma (Fig. 5). All Hf data are shown in the upper plot. Following is a temporal outline of the magmatic evolution, divided into phases that are defined on the basis of changes in U-Pb age and $\varepsilon_{Hf(t)}$ value.

Phase A: This phase includes the earliest magmatism in YTTs, ranging from Late Ordovician (ca. 450 Ma) through mid-Silurian (ca. 422 Ma) time, with a maximum in age probability of 424 Ma. The $\varepsilon_{Hf(t)}$ values are highly juvenile (+7 to +13).

Phase B: Magmatism continued during mid-Silurian through Early Devonian time (ca. 422 to ca. 395 Ma), with a peak in age probability at 407 Ma. The $\varepsilon_{Hf(t)}$ values decrease progressively during this phase, reaching relatively evolved $\varepsilon_{Hf(t)}$ values of –5 to –10 by the end of Early Devonian time (ca. 395 Ma).

Phases C and D: Following a brief lull (ca. 395 to ca. 387 Ma; phase C), magmatism reignited and remained active until just before the end of Devonian time (ca. 363 Ma). The $\varepsilon_{Hf(t)}$ values for this magmatism commence with

highly juvenile values (+10 to +15) during Middle Devonian time (ca. 387 to ca. 375 Ma) and then decrease to moderately juvenile values (+5 to +10) during Late Devonian time (ca. 375 to ca. 363 Ma).

Phases E and F: Following a lull in magmatism during latest Devonian time (ca. 363 to ca. 357 Ma; phase E), magmatism occurred during early Carboniferous time (ca. 357 to ca. 342 Ma) with highly negative $\varepsilon_{Hf(t)}$ values (phase F). This latter magmatism is recorded only in conglomeratic strata along the base of the Port Houghton assemblage, whereas all prior magmatism is recorded in both the Endicott Arm and Port Houghton assemblages.

These variations in $\varepsilon_{Hf(t)}$ values through time are interpreted to record changes in the proportion and/or age of crustal material that was involved in melting during magmatism. Zircons with highly juvenile $\varepsilon_{Hf(t)}$ values (i.e., +15 to +5 $\varepsilon_{Hf(t)}$ for Silurian zircons) must have been produced primarily from melting of mantle material or crustal material that was extracted from the mantle only a short time before magmatic crystallization. In contrast, more negative values (i.e., 0 to –15 $\varepsilon_{Hf(t)}$ for Silurian zircons) record incorporation of significant proportions of older crust, with the extent of the change in $\varepsilon_{Hf(t)}$ value controlled by the age and proportion of incorporated older crust. Alternative explanations for the observed patterns include lateral migration of magmatism such that it incorporated younger (juvenile) versus older (evolved) crust, or stationary magmatism that was generated by melting of mainly juvenile materials during periods of crustal extension (juvenile $\varepsilon_{Hf(t)}$ values) and mainly older crustal materials during crustal thickening (evolved $\varepsilon_{Hf(t)}$ values; e.g., Kemp et al., 2009). These controls, and their implications for the tectonic history of YTTs, are discussed next.

Regional Comparisons of U-Pb and Hf Data

Comparison of YTTs and YTTn

Although many previous studies have suggested that YTTs is related to YTTn/NAa, our new data provide an opportunity to examine possible connections in more detail. Figure 5 (lower panel) provides a comparison of U-Pb ages that have been reported from YTTs and YTTn – unfortunately, only whole-rock Hf data are available for YTTn and no Hf isotopic data are available for NAa. Hf isotopic data for whole-rock metasedimentary samples are similar to the zircon-Hf data reported on Figure 5, with mainly Paleoproterozoic and Archean T_{DM} model ages (Piercey and Colpron, 2009).

Figure 5 (lower panel) shows several different age distribution curves for the northern portion of YTT, including (1) all analyses available from metasedimentary, metavolcanic, and metaplutonic rocks in YTTn and NAa (light red curve; compiled from Colpron et al., 2006; Devine et al., 2006; Mihalynuk et al., 2006; Murphy et al., 2006; Piercey and Colpron, 2009; Dusel-Bacon et al., 2004, 2006, 2013), (2) the age distribution of igneous rocks in YTTn (medium red curve; from fig. 4 *in* Nelson et al., 2006), and (3) the age distribution of igneous rocks in NAa (dark red curve; from fig. 4 *in* Nelson et al., 2006). It should be noted that the pre–360 Ma portion of the age distribution for YTTn is an overestimate because it contains several ages from SE Alaska, and this portion of the curve is marked accordingly on Figure 5.

Comparison of the Precambrian ages in YTTs and YTTn/NAa suggests that they were derived from a similar source region, dominated by rocks of Archean and Paleoproterozoic age. The main difference is the occurrence of a greater proportion of 1.7–1.0 Ga grains in YTTs, which were most likely recycled from the "Grenville clastic wedge" that is interpreted to have covered the Precambrian basement of NW Laurentia during Neoproterozoic time (Rainbird et al., 2012). Although the depositional age of Tracy Arm quartzites is unknown, the occurrence of one sample (87GC420) with predominantly 1.5–1.0 Ga ages raises the possibility that YTTs includes strata that are correlative with Neoproterozoic rocks of northwest Laurentia characterized by a "Grenville clastic wedge" detrital zircon signature (e.g., Lane and Gehrels, 2014). We interpret this sample as part of the Tracy Arm assemblage because it occurs between quartzites (samples 87GC414/12MP33 and 12MP41) that have typical Paleoproterozoic and Archean ages. Two additional samples (Safa and Kah Shakes) apparently contain a mix of grains derived from NW Laurentian basement (>1.7 Ga ages) and from overlying Neoproterozoic strata (1.7–1.0 Ga ages).

Paleozoic ages in YTTs and YTTn/NAa are also similar, especially in the abundance of 380–360 Ma magmatism in YTTs and NAa and 360–340 Ma magmatism in YTTs and YTTn. The primary difference is the presence of Late Ordovician through Early Devonian magmatism in YTTs, which is not represented to the north. This difference was originally noted by Saleeby (2000), who offered the explanation that during early to mid-Paleozoic time, the Yukon-Tanana terrane was part of a west-facing convergent margin system, with YTTs located outboard (west) of YTTn/NAa. Saleeby (2000) suggested that this arc system experienced a history that is common in Cordilleran convergent margin systems, where magmatism migrates inboard over time. Hence, magmatism would have originated first in YTTs during Silurian–Early Devonian time, and then migrated eastward into YTTn/NAa during Middle Devonian through Carboniferous time. Such a model is consistent with the similarity of detrital zircon ages in pre-arc rocks, as noted earlier herein, as well as the complementary nature of mid-Paleozoic magmatism recorded in YTTn/NAa and YTTs. The following evolutionary history compares the U-Pb/Hf data from YTTs with the mid-Paleozoic geologic and geochemical records in YTTn/NAa (Nelson et al., 2006) using the phases defined in this study and the cycles defined by Nelson et al. (2006) (keyed to Fig. 5).

Phases A and B (450–395 Ma): These phases record magmatism within YTTs that predates magmatism in YTTn/NAa. Evolved $\varepsilon_{Hf(t)}$ values document increasing involvement of older crustal materials from mid-Silurian (ca. 422 Ma) through Early Devonian (ca. 395 Ma) time.

Phases C and D (395–363 Ma)–Cycle I (395–365 Ma): This period records abundant magmatism in YTTs beginning at ca. 387 Ma, initiation of magmatism in NAa at ca. 375 Ma, and initiation of magmatism in YTTn at ca. 365 Ma. Magmatism during this period occurred in a regime of regional crustal extension, which is manifest geologically in YTTn, NAa, and the adjacent Cordilleran

passive margin (Nelson et al., 2006), and by the juvenile $\varepsilon_{Hf(t)}$ values for magmatism in YTTs.

Phase E (363–357 Ma)–Cycle II (365–357 Ma): This period marks the end of magmatism within YTTs, a decrease in magmatism in NAa, and the occurrence of felsic magmas of crustal derivation in YTTn (Dusel-Bacon et al., 2006; Nelson et al., 2006). The $\varepsilon_{Hf(t)}$ values in YTTs record a transition during this time period from juvenile values (+5 to +15) before ca. 363 Ma to evolved values (–10 to –20) after ca. 357 Ma. The occurrence of magmas of crustal derivation in YTTn and the reduction in $\varepsilon_{Hf(t)}$ values in YTTs are interpreted to record the onset of an important phase of compression and crustal thickening within the Yukon-Tanana terrane.

Phase F (357–342 Ma)–Cycle III (357–342 Ma): This period records abundant magmatism of crustal affinity associated with widespread deformation, erosion, and accumulation of conglomerates in YTTn (Nelson et al., 2006). Many sections of YTTn and NAa show unconformities and accumulation of conglomeratic strata during this time period (plate 2 of Colpron et al., 2006). Similar evidence of deformation and erosion is preserved in the Port Houghton assemblage of YTTs, where a basal conglomerate rests unconformably on older rocks of the Endicott Arm assemblage and yields detrital zircons with highly evolved $\varepsilon_{Hf(t)}$ values (Fig. 5). Conglomeratic strata of the Port Houghton assemblage were likely derived in large part from YTTn, as magmatism had ceased in the Endicott Arm assemblage prior to this time.

Cycle IV (342–314 Ma): This phase records a change in magmatism within YTTn and YTTs to more mafic compositions, which are not represented in zircon age distributions.

In summary, the interpretation that YTTs has primary affinities with YTTn and NAa is supported by: (1) the occurrence in pre-Devonian passive-margin strata of predominantly 2.8–2.5 Ga and 2.0–1.7 Ga detrital zircons, although this conclusion needs further evaluation given that only one sample has been analyzed from YTTn (Fig. 5); (2) Late Devonian magmatism that is interpreted to be extensional in origin in NAa and YTTn (on the basis of geologic and geochemical relations) as well as in YTTs (on the basis of juvenile $\varepsilon_{Hf(t)}$ values); and (3) the occurrence of Mississippian conglomeratic strata in YTTs (Port Houghton assemblage) and YTTn (Klinkit assemblage) that are coeval, similar lithologically, and interpreted to record episodes of crustal thickening (evidence of deformation, uplift, and erosion in YTTn and YTTs; highly evolved $\varepsilon_{Hf(t)}$ values in YTTs). The primary difference between YTTs and YTTn/NAa is that YTTs contains abundant evidence for Late Ordovician–Silurian–Early Devonian magmatism, which is lacking in YTTn and NAa. Tectonic scenarios that incorporate these similarities, and also the earlier onset of magmatism in YTTs (Saleeby, 2000; Gehrels, 2001), are explored later in the paper.

Comparison of YTTs with Cordilleran Passive-Margin Strata

Our new data also allow us to reevaluate previous suggestions that YTT originated along the northern Cordilleran margin (e.g., Tempelman-Kluit, 1976, 1979; Hansen, 1990; Mortensen, 1992; Dusel-Bacon et al., 2004, 2006, 2013; Nelson et al., 2006, 2013; Piercey and Colpron, 2009). Figure 6 presents a comparison between U-Pb ages and $\varepsilon_{Hf(t)}$ values of Precambrian zircon grains in YTTs and Neoproterozoic through Devonian strata of the Cordilleran passive margin (Gehrels and Pecha, 2014). U-Pb ages are also shown for YTTn and NAa; however, Hf data are not available for the northern assemblages.

This comparison of U-Pb ages (Fig. 6) shows that rocks of the YTT have a strong resemblance with Neoproterozoic through Devonian passive-margin strata that accumulated along the northwestern Laurentian margin. Similarities for YTTs are more pronounced with strata of eastern Alaska and Yukon, whereas similarities for YTTn/NAa are more pronounced with northern British Columbia. The Hf isotopic data also reveal pronounced similarities with strata from northern portions of the Cordilleran passive margin.

Comparison of YTTs with the Alexander Terrane

The Alexander terrane is present outboard of the Yukon-Tanana terrane (Fig. 1) and contains rocks of Neoproterozoic and Paleozoic age. The Alexander terrane is unusual in that its early Paleozoic geologic record changes dramatically along the length of the terrane. In the south, the Alexander terrane consists largely of volcanic, plutonic, and sedimentary rocks that are interpreted to have formed in an oceanic arc-type environment (Gehrels and Saleeby, 1987). Main phases of magmatism occurred during Neoproterozoic (630–550 Ma) and Ordovician–Silurian (490–400 Ma) time. Detrital zircons in clastic strata are almost entirely arc-derived, with few pre–630 Ma grains and juvenile (+15 to +8) $\varepsilon_{Hf(t)}$ values for most zircons (White et al., 2016). To the north, these juvenile arc-type rocks grade into mainly shelf-facies strata that contain both abundant Precambrian detrital zircons and early Paleozoic detrital zircons with highly evolved $\varepsilon_{Hf(t)}$ values (Beranek et al., 2012, 2013a, 2013b).

We consider the Alexander terrane to be an oblique slice through an early Paleozoic convergent-margin system, with continental affinities to the north and oceanic-arc affinities to the south (White et al., 2016). Comparisons between the Alexander terrane and the northern margin of Baltica/Laurentia using geology, faunal affinities, paleolatitudes, U-Pb ages, and Hf isotope signatures suggest that the Alexander terrane formed along the Arctic margin of Baltica/Laurentia and was brought to its present position outboard of the YTT during Mesozoic time (Soja, 1994; Bazard et al., 1995; Gehrels et al., 1996; Butler et al., 1997; Soja and Krutikov, 2008; Colpron and Nelson, 2009, 2011; Miller et al., 2011; Beranek et al., 2012, 2013a, 2013b; Nelson et al., 2013; Tochilin et al., 2014; White et al., 2016). Analysis of the paleogeography and paleomagnetic declinations from the Alexander terrane suggests that the early Paleozoic arc system faced northward, away from Laurentia (fig. 9 of White et al., 2016).

Possible correlations between YTTn and the Alexander terrane have not been explored in most previous syntheses, given that magmatism in the Alexander terrane is mainly Ordovician–Silurian in age, whereas magmatism in YTTn is mainly Late Devonian–Carboniferous in age; however, the documentation of Silurian magmatism in YTTs by Saleeby (2000), Gehrels (2001), and in this study raises the possibility that connections between YTTs and

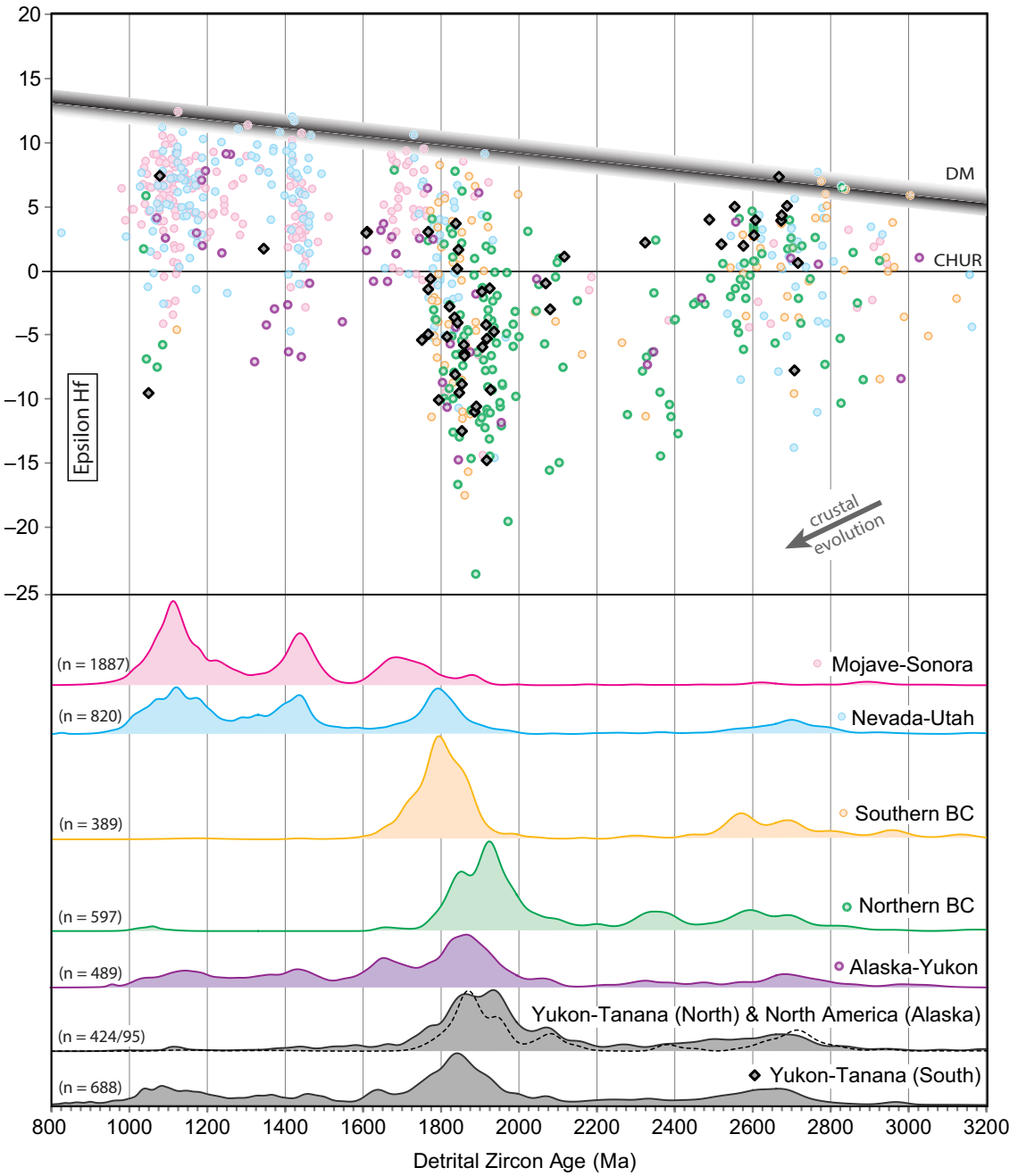

Figure 6. Comparison of age-Hf isotopic information from pre–Late Devonian strata of YTTs, YTTn/NAa, and Cordilleran passive-margin strata. Curve for YTTs is from Tracy Arm assemblage (TAA) strata shown in Figure 5. Curves for YTTn/Na include results from all ages of strata (solid line) and from only pre-Devonian strata (dashed line). Data from pre–Late Devonian strata of the Cordilleran passive-margin sequence are from Gehrels and Pecha (2014), with additional U-Pb ages for Alaska-Yukon from Leslie (2009) and Lane and Gehrels (2014). In upper plot, filled black symbols show values for TAA. Other information on upper panel is from Figure 5. DM—depleted mantle; CHUR—chondritic uniform reservoir.

the Alexander terrane may have existed during early to mid-Paleozoic time. Figure 7 provides a comparison of the U-Pb ages and $\varepsilon_{Hf(t)}$ values from YTTs and both arc-type (SE Alaska) and shelf-facies (Saint Elias Mountains) components of the Alexander terrane. These comparisons show that there are strong similarities in the ages and Hf isotope signatures of zircons in YTTs and in the SE Alaska portion of the Alexander terrane: both assemblages record evolution in juvenile arc systems during Neoproterozoic (630–560 Ma) and Late Ordovician through Early Devonian (460–420 Ma) time, followed by an excursion to more evolved values during Late Devonian–early Mississippian time (Fig. 7). Thus, it is possible for connections to have existed between YTTs and the southern (SE Alaska) portion of the Alexander terrane during early Paleozoic time. In contrast, Neoproterozoic–early Paleozoic magmatism recorded in shelf-facies strata of the northern Alexander terrane is older and consistently more evolved in Hf isotopic signature.

Collectively, the $\varepsilon_{Hf(t)}$ patterns shown in Figure 7 provide a new and potentially powerful record of tectonic processes operating along the northern and northwestern margins of Laurentia during Neoproterozoic–Paleozoic time. Three orogenic phases are recorded, with episodes of crustal thickening (indicated by a progression from juvenile to more-evolved $\varepsilon_{Hf(t)}$ values) occurring during Early Silurian (ca. 440 Ma), latest Early Devonian (ca. 395 Ma), and early Mississippian

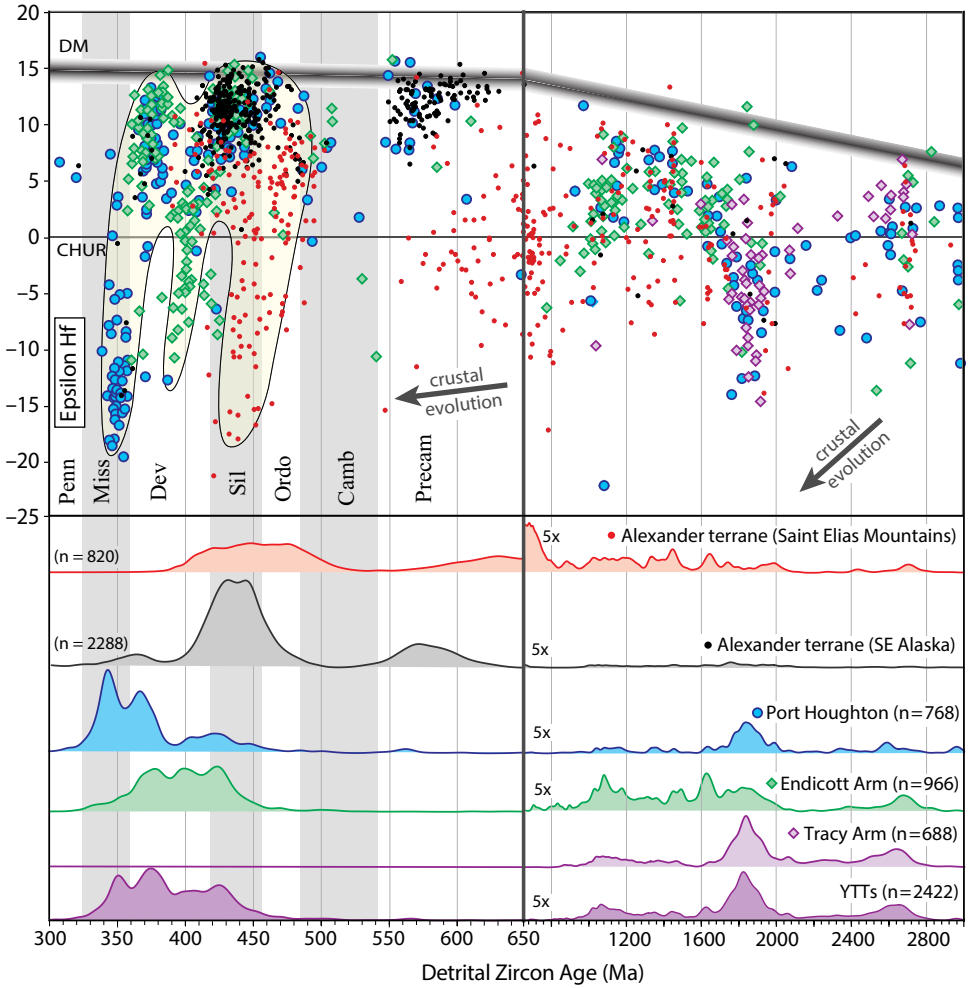

Figure 7. Comparison of age-Hf isotopic data from YTTs and the Alexander terrane. Lower panel shows age-distribution diagrams for different assemblages of YTTs (from Fig. 5), the southeastern Alaska portion of the Alexander terrane (White et al., 2016), and the Saint Elias Mountains portion of the Alexander terrane (Beranek et al., 2012, 2013a, 2013b). Upper panel compares $\varepsilon_{Hf(t)}$ values from the same assemblages. Other information on upper panel is from Figure 5. DM—depleted mantle; CHUR—chondritic uniform reservoir; Penn—Pennsylvanian; Miss—Mississippian; Dev—Devonian; Sil—Silurian; Ordo—Ordovician; Camb—Cambrian; Precam—Precambrian.

(ca. 350 Ma) time (Fig. 7). This apparent ~45 m.y. periodicity in convergent-margin processes is similar to orogenic cycles reported for the Andes (DeCelles et al., 2015) and the Coast Mountains batholith (Gehrels et al., 2009).

Tectonic Synthesis

Figure 8 is a tectonic model that attempts to integrate the new results outlined herein with the large body of work presented by previous researchers.

The oldest units in YTTs, YTTn, and NAa consist of Neoproterozoic–Lower Paleozoic quartz-rich sandstone, limestone, and subordinate fine-grained clastic strata that accumulated in a passive-margin setting. There is widespread agreement that these strata formed along the Cordilleran passive margin, with detritus shed primarily from the northwestern Canadian Shield (Tempelman-Kluit, 1976, 1979; Mortensen, 1992; Hansen, 1990; Nelson et al., 2006, 2013; Dusel-Bacon et al., 2004, 2006, 2013; Piercey and Colpron, 2009), and perhaps from Neoproterozoic strata of the Grenville clastic wedge (Rainbird et al., 2012). Comparison of available U-Pb ages suggests that YTTn/NAa have the closest affinity with passive-margin strata in northern British Columbia, whereas YTTs is matched best with strata from eastern Alaska and Yukon (Fig. 6).

Magmatism commenced in YTTs during Late Ordovician–Silurian time (phase A; Fig. 8A) with juvenile $\varepsilon_{Hf(t)}$ values (Fig. 5). These juvenile values overlap with the ages and Hf isotopic signatures of detrital zircons and igneous rocks that occur in the SE Alaska portion of the Alexander terrane (White et al., 2016). This raises the possibility that Ordovician–Silurian magmatism within YTTs occurred along the same convergent margin system as the Alexander terrane, which was apparently located along the paleo-Arctic margin of Baltica and/or Laurentia during early Paleozoic time (Soja, 1994; Bazard et al., 1995; Gehrels et al., 1996; Butler et al., 1997; Soja and Krutikov, 2008; Colpron and Nelson, 2009, 2011; Miller et al., 2011; Beranek et al., 2012, 2013a, 2013b; Nelson et al., 2013; White et al., 2016). The occurrence in both YTTs and the southern Alexander terrane of 630–560 Ma and 450–410 Ma zircons with juvenile $\varepsilon_{Hf(t)}$ values, and 380–340 Ma zircons with rapidly decreasing $\varepsilon_{Hf(t)}$ values (Fig. 7), further supports the possibility that Ordovician–Silurian magmatism within YTTs occurred along the same convergent margin system as the Alexander terrane. Other terranes that may have been associated with this convergent margin system include the Pearya terrane (Hadlari et al., 2014; Malone, 2012; Malone et al., 2014) and "Crockerland" (Anfinson et al., 2012) along the Franklinian (northern Laurentian) margin, the Farewell terrane of central Alaska (Malkowski and Hampton, 2014), and the Arctic Alaska–Chukotka terrane of northern Alaska–northern Siberia (Miller et al., 2011). Interestingly, strata in the Saint Elias Mountains (northern) portion of the Alexander terrane, which, like YTT, have continental margin affinities, have an age-Hf pattern (Beranek et al., 2012, 2013a, 2013b) that is quite different from YTTs and the southern Alexander terrane (Fig. 7). The inset map of Figure 8 shows a possible configuration of YTT and the Alexander terrane along this convergent margin system.

Magmatism within YTTs continued during Early Devonian time (phase B; Fig. 8B), but with progressively more negative $\varepsilon_{Hf(t)}$ values (Fig. 5). This Hf isotopic pull-down is interpreted to record ca. 422–395 Ma crustal thickening within YTTs given that there is no evidence of the arc migrating into older crust during this time.

Following a late Early and early Middle Devonian magmatic lull in YTTs (phase C; early cycle I), a significant phase of Middle to Late Devonian magmatism with juvenile $\varepsilon_{Hf(t)}$ values occurred in YTTs (Phase D; late cycle I; Fig. 8C). Late Devonian magmatism commenced to the north, first in NAa and then in YTTn, in an extensional tectonic setting.

A major change occurred during latest Devonian time (phase E; cycle II; Fig. 8D) with cessation of magmatism in YTTs, waning magmatism in NAa, and the onset of voluminous magmatism in YTTn. This continued during early Mississippian time (phase F; cycle III; Fig. 8D) with widespread deformation, uplift, erosion, accumulation of conglomeratic strata, and generation of crustal melts in YTTn (Nelson et al., 2006). There are no early Mississippian igneous rocks in YTTs, but detrital zircons of this age, with highly evolved $\varepsilon_{Hf(t)}$ values (Fig. 5), are abundant in conglomeratic strata along the unconformable base of the Port Houghton assemblage. We accordingly suggest that conglomeratic strata in the Port Houghton assemblage were shed from YTTn, where there is strong evidence of magmatism occurring during deformation, erosion, and presumably crustal thickening (Fig. 8D).

Regionally, YTTn and YTTs are interpreted to have rifted away from the Cordilleran margin beginning in latest Devonian to early Mississippian time, opening the Slide Mountain ocean basin inboard of YTTn/s (Fig. 8E). Rocks of NAa are interpreted to have remained on the inboard side of the Slide Mountain ocean basin, ending their primary connection with YTTn/s (Dusel-Bacon et al., 2004, 2006; Nelson et al., 2006, 2013).

Magmatism within YTTn is interpreted to have waned during mid-Mississippian time, with accumulation of mainly basinal strata, mafic volcanic rocks of arc and back-arc affinity, and only local felsic volcanic rocks (Fig. 8E). This basinal arc and back-arc environment is recorded in YTTn through Early Permian time, until subduction polarity apparently switched during Late Permian time, and YTTn began to migrate eastward (Fig. 8F), eventually colliding with the Cordilleran margin during latest Permian–Early Triassic time (Fig. 8G; Nelson et al., 2006, 2013; Beranek and Mortensen, 2011). The record preserved within YTTs ends in Carboniferous time, although it is likely that Carboniferous and Permian strata of the adjacent Taku terrane (Fig. 1) originally formed the uppermost part of YTTs (Gehrels, 2002; Giesler et al., 2016).

We interpret YTTs to have been located along the outboard margin of, or north of, YTTn/NAa through Middle Jurassic time (Figs. 8A–8G). Displacement of YTTs southward relative to YTTn/NAa is suggested to have occurred during Late Jurassic–Early Cretaceous time, when sinistral faults were active in the northern Cordillera (Monger et al., 1994), and there was a sinistral component of plate motion along the Cordilleran margin (Engebretson et al., 1985). Gehrels et al. (2009) suggested that one of these faults occurred within YTT, bringing rocks of YTTs ~1000 km southward relative to YTTn/NAa and to their present position outboard of the Stikine terrane (Fig. 1). Other faults in this set may have included a sinistral fault that juxtaposed northern/outboard and southern/

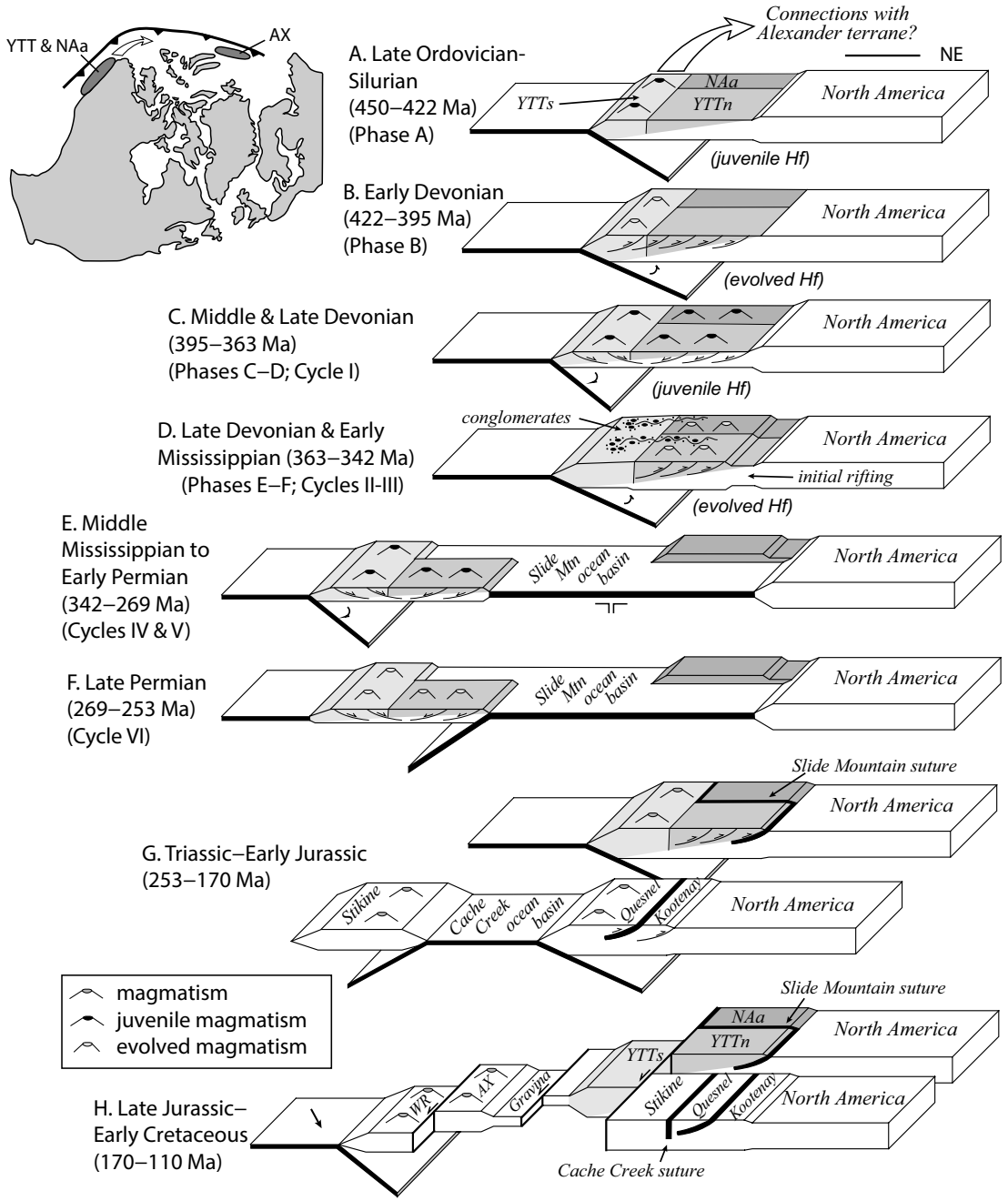

Figure 8. Schematic tectonic model showing our proposed evolution of the Yukon-Tanana terrane (YTT) and related assemblages along the northern Cordilleran margin. See "Tectonic Synthesis" section of the text for explanation. Inset map shows possible location of YTT/NAa and the Alexander terrane (AX) along the same subduction system during Silurian time (adapted from Miller et al., 2011; Nelson et al., 2013; White et al., 2016). YTTs—SE Alaska subterrane of the Yukon-Tanana terrane; WR—Wrangellia.

inboard portions of the Gravina basin (Yokelson et al., 2015), and a sinistral fault that brought the Banks Island assemblage of the Alexander terrane and the Vancouver Island portion of Wrangellia southward to their present positions (Tochilin et al., 2014). This sinistral-emplacement hypothesis is offered as an alternative to the view that YTTs formed along the outboard margin of the Stikine terrane (Nelson et al., 2006, 2013) and that both YTTs and Stikine were brought to their present position by counterclockwise oroclinal rotation away from the northern Cordilleran margin (Mihalynuk et al., 1994; Nelson et al., 2013; Colpron et al., 2015).

CONCLUSIONS

One of the main conclusions from our study is that the SE Alaska subterrane of the Yukon-Tanana terrane (YTTs) has strong similarities with northern portions of the Yukon-Tanana terrane (YTTn) and pericratonic strata in eastern Alaska (NAa). These similarities include overlapping ages of Precambrian detrital zircons in Neoproterozoic–Lower Paleozoic pericratonic strata (Fig. 6) and complementary histories of mid-Paleozoic arc-type magmatism (Fig. 5). The strongest similarities in magmatic history are during Late Devonian through early Mississippian time, when stratigraphic and geochemical relations in YTTn and Hf isotopic values in YTTs are interpreted to record a transition from extensional to compressional magmatism (Figs. 8C–8D).

Rocks in YTTs also record Late Ordovician through Early Devonian magmatism that is not recorded in YTTn/NAa. This magmatism records a parallel trend from extensional to compressional magmatism (Figs. 8A–8B), with juvenile $\varepsilon_{Hf(t)}$ values for Late Ordovician and Silurian zircons and more-evolved values for Early Devonian grains (Fig. 5). The occurrence of juvenile magmatism during Silurian time in YTTs, as well as in the Alexander (White et al., 2016), Farewell (Malkowski and Hampton, 2014), and possibly Arctic Alaska–Chukotka (Miller et al., 2011) and Franklinian (Anfinson et al., 2012; Hadlari et al., 2014) terranes, suggests that all of this magmatism may have occurred along the same convergent margin system (see inset map of Fig. 8).

The similarities and differences noted here suggest that it is appropriate to refer to YTTs and YTTn as different subterranes of the Yukon-Tanana terrane, and this is consistent with Saleeby's (2000) hypothesis that YTTs may have been located along the outboard margin of YTTn. Alternatively, YTTs may have been located along strike of YTTn on the northern or northwestern Laurentian margin during its earlier history. These comparisons also demonstrate the power of coupled U-Pb/Hf data for tectonic analysis and suggest that such data from other Cordilleran terranes will be helpful in reconstructing their origins and displacement histories.

ACKNOWLEDGMENTS

The National Science Foundation (NSF) is acknowledged for support of this project (NSF grants EAR-0947904 and EAR-0948359) and for support of the Arizona LaserChron Center (grant EAR-1338583). We thank Clayton Loehn, Kenneth Kanipe, Gayland Simpson, Beth Welke, Ryan Graham, and Cooper Kowalski for their technical support in helping to prepare the zircon separates and acquiring the scanning electron microscope images. We thank Peter G. DeCelles for his critical insights, which greatly improved the quality of this manuscript. We also acknowledge Captain Don Willson for sharing his nautical expertise and logistical support while navigating the waters of southeast Alaska. L. Beranek and J. Nelson provided exceptionally thorough and helpful reviews of this manuscript.

REFERENCES CITED

Alldrick, D.J., Friedman, R.M., and Childe, F.C., 2001, Age and Geologic History of the Ecstall Greenstone Belt, Northwest British Columbia: Geological Fieldwork 2000: British Columbia Geological Survey Paper 2001–1, p. 269–278.

Amelin, Y., Lee, D.C., Halliday, A.N., and Pidgeon, R.T., 1999, Nature of the Earth's earliest crust from Hf isotopes in single detrital grains: Nature, v. 399, p. 252–255, doi:10.1038/20426.

Amelin, Y., Lee, D.-C., and Halliday, A.N., 2000, Early-middle Archean crustal evolution deduced from Lu-Hf and U-Pb isotopic studies of single zircon grains: Geochimica et Cosmochimica Acta, v. 64, no. 24, p. 4205–4225, doi:10.1016/S0016-7037(00)00493-2.

Anfinson, O.A., Leier, A.L., Gaschnig, R., Embry, A.F., and Dewing, K., 2012, U-Pb and Hf isotopic data from Franklinian Basin strata: Insights into the nature of Crockerland and the timing of accretion, Canadian Arctic Islands: Canadian Journal of Earth Sciences, v. 49, p. 1316–1328, doi:10.1139/e2012-067.

Bazard, D.R., Butler, R.F., Gehrels, G.E., and Soja, C.M., 1995, Early Devonian paleomagnetic data from the Lower Devonian Karheen Formation suggest Laurentia-Baltica connection for the Alexander terrane: Geology, v. 23, p. 707–710, doi:10.1130/0091-7613(1995)023<0707:EDPDFT>2.3.CO;2.

Beranek, L.P., and Mortensen, J.K., 2011, The timing and provenance record of the Late Permian Klondike orogeny in northwestern Canada and arc-continent collision along western North America: Tectonics, v. 30, TC5017, doi:10.1029/2010TC002849.

Beranek, L.P., van Staal, C.R., Gordee, S.M., McClelland, W.C., Israel, S., and Mihalynuk, M.G., 2012, Tectonic significance of Upper Cambrian–Middle Ordovician mafic volcanic rocks on the Alexander terrane, Saint Elias Mountains, northwestern Canada: The Journal of Geology, v. 120, p. 293–314, doi:10.1086/664788.

Beranek, L.P., van Staal, C.R., McClelland, W.C., Israel, S., and Mihalynuk, M.G., 2013a, Baltican crustal provenance for Cambrian–Ordovician sandstones of the Alexander terrane, North American Cordillera: Evidence from detrital zircon U-Pb geochronology and Hf isotope geochemistry: Journal of the Geological Society of London, v. 170, p. 7–18, doi:10.1144/jgs2012-028.

Beranek, L.P., van Staal, C.R., McClelland, W.C., Israel, S., and Mihalynuk, M.G., 2013b, Detrital zircon Hf isotopic compositions indicate a northern Caledonian connection for the Alexander terrane: Lithosphere, v. 5, no. 2, p. 163–168, doi:10.1130/L255.1.

Berg, H.C., Jones, D.L., and Coney, P.J., 1978, Map Showing Pre-Cenozoic Tectonostratigraphic Terranes of Southeastern Alaska and Adjacent Areas: U.S. Geological Survey Open-File Report 78–1085, scale 1:1,000,000.

Bouvier, A., Vervoort, J.D., and Patchett, J.D., 2008, The Lu-Hf and Sm-Nd isotopic composition of CHUR: Constraints from unequilibrated chondrites and implications for the bulk composition of terrestrial planets: Earth and Planetary Science Letters, v. 273, p. 48–57, doi:10.1016/j.epsl.2008.06.010.

Butler, R.F., Gehrels, G.E., and Bazard, D.R., 1997, Paleomagnetism of Paleozoic strata of the Alexander terrane, southeastern Alaska: Geological Society of America Bulletin, v. 109, no. 10, p. 1372–1388, doi:10.1130/0016-7606(1997)109<1372:POPSOT>2.3.CO;2.

Cecil, R., Gehrels, G., Patchett, J., and Ducea, M., 2011, U-Pb-Hf characterization of the central Coast Mountains batholith: Implications for petrogenesis and crustal architecture: Lithosphere, v. 3, no. 4, p. 247–260, doi:10.1130/L134.1.

Cohen, K.M., Finney, S.C., Gibbard, P.L., and Fan, J.-X., 2013, The ICS International Chronostratigraphic Chart (updated): Episodes, v. 36, p. 199–204.

Colpron, M., and Nelson, J.L., eds., 2006, Paleozoic Evolution and Metallogeny of Pericratonic Terranes at the Ancient Pacific Margin of North America, Canadian and Alaskan Cordillera: Geological Association of Canada Special Paper 45, 523 p.

Colpron, M., and Nelson, J., 2009, A Paleozoic Northwest Passage: Incursion of Caledonian, Baltican and Siberian terranes into eastern Panthalassa, and the early evolution of the North American Cordillera, *in* Cawood, P.A., and Kroner, A., eds., Earth Accretionary Systems in Space and Time: The Geological Society London Special Publication 318, p. 273–307.

Colpron, M., and Nelson, J., 2011, A Paleozoic NW Passage and the Timanian, Caledonian and Uralian connections of some exotic terranes in the North American Cordillera, *in* Spencer,

A.M., Embry, A.F., Gautier, D.L., Stoupakova, A.V., and Sorensen, K., eds., Arctic Petroleum Geology: Geological Society of London Memoir 35, p. 463–484.

Colpron, M., Nelson, J.L., and Murphy, D.C., 2006, A tectonostratigraphic framework for the pericratonic terranes of the northern Canadian Cordillera, *in* Colpron, M., and Nelson, J.L., eds., Paleozoic Evolution and Metallogeny of Pericratonic Terranes at the Ancient Pacific Margin of North America, Canadian and Alaskan Cordillera: Geological Association of Canada Special Paper 45, p. 1–23.

Colpron, M., Crowley, J., Gehrels, G., Long, D., Murphy, D., Beranek, L., and Bickerton, L., 2015, Birth of the northern Cordilleran orogen, as recorded by detrital zircons in Jurassic synorogenic strata and regional exhumation in Yukon: Lithosphere, v. 7, no. 5, p. 541–562, doi:10.1130/L451.1.

Coney, P.J., Jones, D.L., and Monger, J.W.H., 1980, Cordilleran suspect terranes: Nature, v. 288, p. 329–333, doi:10.1038/288329a0.

DeCelles, P., Zandt, G., Beck, S., Currie, C., Ducea, M., Kapp, P., Gehrels, G., Carrapa, B., Quade, J., and Schoenbohm, L., 2015, Cyclical orogenic processes in the Cenozoic central Andes, *in* DeCelles, P.G., Ducea, M.N., Carrapa, B., and Kapp, P.A., eds., Geodynamics of a Cordilleran Orogenic System: The Central Andes of Argentina and Northern Chile: Geological Society of America Memoir 212, p. 459–490, doi:10.1130/2015.1212(22).

Devine, F., Carr, S.D., Murphy, D.C., Davis, W.J., Smith, S., and Villeneuve, M.E., 2006, Geochronological and geochemical constraints on the origin of the Klatsa metamorphic complex: Implications for early Mississippian high-pressure metamorphism within Yukon-Tanana terrane, *in* Colpron, M., and Nelson, J.L., eds., Paleozoic Evolution and Metallogeny of Pericratonic Terranes at the Ancient Pacific Margin of North America, Canadian and Alaskan Cordillera: Geological Association of Canada Special Paper 45, p. 107–130.

Dusel-Bacon, C., Wooden, J.L., and Hopkins, M.J., 2004, U-Pb zircon and geochemical evidence for bimodal mid-Paleozoic magmatism and syngenetic base-metal mineralization in the Yukon-Tanana terrane, Alaska: Geological Society of America Bulletin, v. 116, no. 7–8, p. 989–1015, doi:10.1130/B25342.1.

Dusel-Bacon, C., Hopkins, M.J., Mortensen, J.K., Dashevsky, S.S., Bressler, J.R., and Day, W.C., 2006, Paleozoic tectonic and metallogenic evolution of the pericratonic rocks of east-central Alaska and adjacent Yukon, *in* Colpron, M., and Nelson, J.L., eds., Paleozoic Evolution and Metallogeny of Pericratonic Terranes at the Ancient Pacific Margin of North America, Canadian and Alaskan Cordillera: Geological Association of Canada Special Paper 45, p. 25–74.

Dusel-Bacon, C., Day, W.C., and Aleinikoff, J.N., 2013, Geochemistry, petrography, and zircon U-Pb geochronology of Paleozoic metaigneous rocks in the Mount Veta area of east-central Alaska: Implications for the evolution of the westernmost part of the Yukon-Tanana terrane: Canadian Journal of Earth Sciences, v. 50, no. 8, p. 826–846, doi:10.1139/cjes-2013-0004.

Engebretson, D.C., Cox, A., and Gordon, R.G., 1985, Relative Motions Between Oceanic and Continental Plates in the Pacific Basin: Geological Society of America Special Paper 206, 60 p., doi:10.1130/SPE206-p1.

Gareau, S.A., and Woodsworth, G.J., 2000, Yukon-Tanana terrane in the Scotia-Quaal belt, Coast plutonic complex, central-western British Columbia, *in* Stowell, H.H., and McClelland, W.C., eds., Tectonics of the Coast Mountains, Southeast Alaska and Coastal British Columbia: Geological Society of America Special Paper 343, p. 23–43, doi:10.1130/0-8137-2343-4.23.

Gehrels, G.E., 2000, Geology and U-Pb geochronology of the western flank of the Coast Mountains between Juneau and Skagway, southeast Alaska, *in* Stowell, H.H., and McClelland, W.C., eds., Tectonics of the Coast Mountains, Southeast Alaska and Coastal British Columbia: Geological Society of America Special Paper 343, p. 213–233.

Gehrels, G.E., 2001, Geology of the Chatham Sound region, southeast Alaska and coastal British Columbia: Canadian Journal of Earth Sciences, v. 38, p. 1579–1599, doi:10.1139/e01-040.

Gehrels, G.E., 2002, Detrital zircon geochronology of the Taku terrane, southeast Alaska: Canadian Journal of Earth Sciences, v. 39, p. 921–931, doi:10.1139/e02-002.

Gehrels, G., 2012, Detrital zircon U-Pb geochronology: Current methods and new opportunities, *in* Busby, C., and Azor, A., eds., Tectonics of Sedimentary Basins: Recent Advances: Wiley-Blackwell Publishing, p. 45–62, doi:10.1002/9781444347166.ch2.

Gehrels, G.E., 2014, Detrital zircon U-Pb geochronology applied to tectonics: Annual Review of Earth and Planetary Sciences, v. 42, p. 127–149, doi:10.1146/annurev-earth-050212-124012.

Gehrels, G.E., and Berg, H.C., 1992, Geologic Map of Southeastern Alaska: U.S. Geological Survey Miscellaneous Investigations Map I-1867, 24 p.

Gehrels, G.E., and Kapp, P.A., 1998, Detrital zircon geochronology and regional correlation of metasedimentary rocks in the Coast Mountains, southeastern Alaska: Canadian Journal of Earth Sciences, v. 35, p. 269–279, doi:10.1139/e97-114.

Gehrels, G.E., and Pecha, M.E., 2014, Detrital zircon U-Pb geochronology and Hf isotope geochemistry of Paleozoic and Triassic passive margin strata of western North America: Geosphere, v. 10, no. 1, p. 49–65, doi:10.1130/GES00889.1.

Gehrels G.E., and Saleeby, J.B., 1987, Geological framework, tectonic evolution, and displacement of the Alexander terrane: Tectonics, v. 6, no. 2, p. 151–173.

Gehrels, G.E., McClelland, W.C., Samson, S.D., and Patchett, P.J., 1991, U Pb geochronology of detrital zircons from a continental margin assemblage in the northern Coast Mountains, southeastern Alaska: Canadian Journal of Earth Sciences, v. 28, p. 1285–1300, doi:10.1139/e91-114.

Gehrels, G.E., McClelland, W.C., Samson, S.D., Patchett, P.J., and Orchard, M.J., 1992, Geology of the western flank of the Coast Mountains between Cape Fanshaw and Taku Inlet, southeastern Alaska: Tectonics, v. 11, no. 3, p. 567–585, doi:10.1029/92TC00482.

Gehrels, G.E., Butler, R.F., and Bazard, D.R., 1996, Detrital zircon geochronology of the Alexander terrane, southeastern Alaska: Geological Society of America Bulletin, v. 108, p. 722–734, doi:10.1130/0016-7606(1996)108<0722:DZGOTA>2.3.CO;2.

Gehrels, G.E., Valencia, V., and Ruiz, J., 2008, Enhanced precision, accuracy, efficiency, and spatial resolution of U-Pb ages by laser ablation–multicollector–inductively coupled plasma–mass spectrometry: Geochemistry Geophysics Geosystems, v. 9, Q03017, doi:10.1029/2007GC001805.

Gehrels, G.E., Rusmore, M., Woodsworth, G., Crawford, M., Andronicos, C., Hollister, L., Patchett, J., Ducea, M., Butler, R., Klepis, K., Davidson, C., Friedman, R., Haggart, J., Mahoney, B., Crawford, W., Pearson, D., and Girardi, J., 2009, U-Th-Pb geochronology of the Coast Mountains batholith in north-coastal British Columbia: Constraints on age and tectonic evolution: Geological Society of America Bulletin, v. 121, p. 1341–1361, doi:10.1130/B26404.1.

Giesler, D., Gehrels, G., Pecha, M., White, C., Yokelson, I., and McClelland, W., 2016, U-Pb and Hf isotopic analyses of detrital zircons from the Taku terrane, southeast Alaska: Canadian Journal of Earth Sciences (in press), doi:10.1139/cjes-2015-0240.

Hadlari, T., Davis, W.J., and Dewing, K., 2014, A pericratonic model for the Pearya terrane as an extension of the Franklinian margin of Laurentia, Canadian Arctic: Geological Society of America Bulletin, v. 126, p. 182–200, doi:10.1130/B30843.1.

Hansen, V.L., 1990, Yukon-Tanana terrane: A partial acquittal: Geology, v. 18, p. 365–369, doi:10.1130/0091-7613(1990)018<0365:YTTAPA>2.3.CO;2.

Kemp, A.I.S., Hawkesworth, C.J., Collins, W.J., Gray, C.M., and Blevin, P.L., 2009, Isotopic evidence for rapid continental growth in an extensional accretionary orogen: The Tasmanides, eastern Australia: Earth and Planetary Science Letters, v. 284, p. 455–466, doi:10.1016/j.epsl.2009.05.011.

Lane, L.S., and Gehrels, G.E., 2014, Detrital zircon lineages of late Neoproterozoic and Cambrian strata, NW Laurentia: Geological Society of America Bulletin, v. 126, no. 3–4, p. 398–414, doi:10.1130/B30848.1.

Leslie, C.D., 2009, Detrital Zircon Geochronology and Rift-Related Magmatism: Central Mackenzie Mountains, Northwest Territories [M.Sc. thesis]: Vancouver, British Columbia, Canada, University of British Columbia, 236 p. (https://open.library.ubc.ca/clRcle/collections/ubctheses/24/items/1.0052744).

Malkowski, M.A., and Hampton, B.A., 2014, Sedimentology, U-Pb detrital geochronology, and Hf isotopic analyses from Mississippian–Permian stratigraphy of the Mystic subterrane, Farewell terrane, Alaska: Lithosphere, v. 6, no. 5, p. 383–398, doi:10.1130/L365.1.

Malone, S.J., 2012, Tectonic Evolution of Northern Ellesmere Island: Insights from the Pearya Terrane, Ellesmerian Clastic Wedge and Sverdrup Basin [Ph.D. thesis]: Iowa City, Iowa, University of Iowa, 276 p., http://ir.uiowa.edu/etd/3496.

Malone, S.J., McClelland, W.C., von Gosen, W., and Piepjohn, K., 2014, Proterozoic evolution of the North Atlantic–Arctic Caledonides: Insights from detrital zircon analysis of metasedimentary rocks from the Pearya terrane, Canadian High Arctic: The Journal of Geology, v. 122, no. 6, p. 623–647, doi:10.1086/677902.

McClelland, W.C., and Mattinson, J.M., 2000, Cretaceous–Tertiary evolution of the western Coast Mountains, central southeastern Alaska, *in* Stowell, H.H., and McClelland, W.C., eds., Tectonics of the Coast Mountains, Southeastern Alaska and British Columbia: Geological Society of America Special Paper 343, p. 159–182, doi:10.1130/0-8137-2343-4.159.

McClelland, W.C., Gehrels, G.E., Samson, S.D., and Patchett, P.J., 1992, Protolith relations of the Gravina belt and Yukon-Tanana terrane in central southeastern Alaska: The Journal of Geology, v. 100, p. 107–123, doi:10.1086/629574.

McClelland, W.C., Gehrels, G.E., Samson, S.D., and Patchett, P.J., 1992, Structural and geochronologic relations along the western flank of the Coast Mountains batholith: Stikine

River to Cape Fanshaw, central southeastern Alaska: Journal of Structural Geology, v. 14, p. 475–489, doi:10.1016/0191-8141(92)90107-8.
Mihalynuk, M.G., Nelson, J., and Diakow, L.J., 1994, Cache Creek entrapment: Oroclinal paradox within the Canadian Cordillera: Tectonics, v. 13, no. 3, p. 575–595, doi:10.1029/93TC03492.
Mihalynuk, M.G., Friedman, R.M., Devine, F., and Heaman, L.M., 2006, Protolith age and deformation history of the Big Salmon complex, relicts of a Paleozoic continental arc in northern British Columbia, *in* Colpron, M., and Nelson, J.L., eds., Paleozoic Evolution and Metallogeny of Pericratonic Terranes at the Ancient Pacific Margin of North America, Canadian and Alaskan Cordillera: Geological Association of Canada Special Paper 45, p. 179–200.
Miller, E.L., Kuznetsov, N., Soboleva, A., Udoratina, O., Grove, M.J., and Gehrels, G.E., 2011, Baltica in the Cordillera?: Geology, v. 39, p. 791–794, doi:10.1130/G31910.1.
Monger, J.W.H., and Berg, H.C., 1987, Lithotectonic Terrane Map of Western Canada and Southeastern Alaska: U.S. Geological Survey Miscellaneous Field Studies Map MF-1874-B, scale 1:2,500,000.
Monger, J.W.H., van der Heyden, P., Journeay, J.M., Evenchick, C.A., and Mahoney, J.B., 1994, Jurassic–Cretaceous basins along the Canadian Coast Belt: Their bearing on pre–mid-Cretaceous sinistral displacements: Geology, v. 22, p. 175–178, doi:10.1130/0091-7613(1994)022<0175:JCBATC>2.3.CO;2.
Mortensen, J.K., 1992, Pre–mid-Mesozoic tectonic evolution of the Yukon-Tanana terrane, Yukon and Alaska: Tectonics, v. 11, no. 4, p. 836–853, doi:10.1029/91TC01169.
Murphy, D.C., Mortensen, J.K., Piercey, S.J., Orchard, M.J., and Gehrels, G.E., 2006, Mid-Paleozoic to early Mesozoic tectonostratigraphic evolution of Yukon-Tanana and Slide Mountain terranes and affiliated overlap assemblages, Finlayson Lake massive sulphide district, southeastern Yukon, *in* Colpron, M., and Nelson, J.L., eds., Paleozoic Evolution and Metallogeny of Pericratonic Terranes at the Ancient Pacific Margin of North America, Canadian and Alaskan Cordillera: Geological Association of Canada Special Paper 45, p. 75–105.
Nelson, J.A., and Gehrels, G., 2007, Detrital zircon geochronology and provenance of the southeastern Yukon-Tanana terrane: Canadian Journal of Earth Sciences, v. 44, p. 297–316, doi:10.1139/e06-105.
Nelson, J.L., Colpron, M., Piercey, S.J., Dusel-Bacon, C., Murphy, D.C., and Roots, C.F., 2006, Paleozoic tectonic and metallogenic evolution of pericratonic terranes in Yukon, northern British Columbia, and eastern Alaska, *in* Colpron, M., and Nelson, J.L., eds., Paleozoic Evolution and Metallogeny of Pericratonic Terranes at the Ancient Pacific Margin of North America, Canadian and Alaskan Cordillera: Geological Association of Canada Special Paper 45, p. 323–360.
Nelson, J.L., Colpron, M., and Israel, S., 2013, The Cordillera of British Columbia, Yukon, and Alaska: Tectonics and Metallogeny, *in* Colpron, M., Bissig, T., Rusk, B.G., and Thompson, J.F.H., eds., Tectonics, Metallogeny, and Discovery: The North American Cordillera and Similar Accretionary Settings: Society of Economic Geologists Special Publication 17, p. 53–109.
Piercey, S.J., and Colpron, M., 2009, Composition and provenance of the Snowcap assemblage, basement to the Yukon-Tanana terrane, northern Cordillera: Implications for Cordilleran crustal growth: Geosphere, v. 5, p. 439–464, doi:10.1130/GES00505.1.
Piercey, S.J., Murphy, C.C., Mortensen, J.K., and Creaser, R.A., 2004, Mid-Paleozoic initiation of the northern Cordilleran marginal backarc basin: Geologic, geochemical, and neodymium isotope evidence from the oldest mafic magmatic rocks in the Yukon-Tanana terrane, Finlayson Lake district, southeast Yukon, Canada: Geological Society of America Bulletin, v. 116, no. 9/10, p. 1087–1106.
Piercey, S.J., Nelson, J.L., Colpron, M., Dusel-Bacon, C., Simard, R.-L., and Roots, C.F., 2006, Paleozoic tectonic and metallogenic evolution of pericratonic terranes in Yukon, northern British Columbia, and eastern Alaska, *in* Colpron, M., and Nelson, J.L., eds., Paleozoic Evolution and Metallogeny of Pericratonic Terranes at the Ancient Pacific Margin of North America, Canadian and Alaskan Cordillera: Geological Association of Canada Special Paper 45, p. 281–322.
Rainbird, R., Cawood, P., and Gehrels, G., 2012, The Great Grenvillian sedimentation episode: Record of supercontinent Rodinia's assembly, *in* Busby, C., and Azor, A., eds., Tectonics of Sedimentary Basins: Recent Advances: Wiley-Blackwell Publishing, p. 583–601, doi:10.1002/9781444347166.ch29.
Rubatto, D., 2002, Zircon trace element geochemistry: Partitioning with garnet and the link between U-Pb ages and metamorphism: Chemical Geology, v. 184, p. 123–138, doi:10.1016/S0009-2541(01)00355-2.
Rubin, C.M., and Saleeby, J.B., 1991, Tectonic framework of the Upper Paleozoic and Lower Mesozoic Alava sequence: A revised view of the polygenetic Taku terrane in southern southeast Alaska: Canadian Journal of Earth Sciences, v. 28, p. 881–893, doi:10.1139/e91-080.
Rubin, C.M., and Saleeby, J.B., 1992, Tectonic history of the eastern edge of the Alexander terrane, southeast Alaska: Tectonics, v. 11, p. 586–602, doi:10.1029/91TC02182.
Rubin, C.M., Miller, M.M., and Smith, G.M., 1990, Tectonic development of mid-Paleozoic volcanic-plutonic complexes: Evidence for convergent margin tectonism, *in* Harwood, D.S., and Miller, M., eds., Paleozoic and Early Mesozoic Paleogeographic Relations; Sierra Nevada, Klamath Mountains, and Related Terranes: Geological Society of America Special Paper 255, p. 1–16, doi:10.1130/SPE255-p1.
Saleeby, J.B., 2000, Geochronologic investigations along the Alexander-Taku terrane boundary, southern Revillagigedo Island to Cape Fox areas, southeast Alaska, *in* Stowell, H.H., and McClelland, W.C., eds., Tectonics of the Coast Mountains, Southeastern Alaska and British Columbia: Geological Society of America Special Paper 343, p. 107–143, doi:10.1130/0-8137-2343-4.107.
Soja, C.M., 1994, Significance of Silurian stromatolite-sphinctozoan reefs: Geology, v. 22, p. 355–358, doi:10.1130/0091-7613(1994)022<0355:SOSSSR>2.3.CO;2.
Soja, C.M., and Krutikov, L., 2008, Provenance, depositional setting, and tectonic implications of Silurian polymictic conglomerates in Alaska's Alexander terrane, *in* Blodgett, R., and Stanley, G., eds., The Terrane Puzzle: New Perspectives on Paleontology and Stratigraphy from the North American Cordillera: Geological Society of America Special Paper 442, p. 63–75, doi:10.1130/2008.442(04).
Stowell, H.H., and Crawford, M.L., 2000, Metamorphic history of the Coast Mountains orogeny, western British Columbia and southeastern Alaska, *in* Stowell, H.H., and McClelland, W.C., eds., Tectonics of the Coast Mountains, Southeastern Alaska and British Columbia: Geological Society of America Special Paper 343, p. 257–283, doi:10.1130/0-8137-2343-4.257.
Tempelman-Kluit, D.J., 1976, The Yukon crystalline terrane: Enigma in the Canadian Cordillera: Geological Society of America Bulletin, v. 87, p. 1343–1357, doi:10.1130/0016-7606(1976)87<1343:TYCTEI>2.0.CO;2.
Tempelman-Kluit, D.J., 1979, Transported Cataclasite, Ophiolite and Granodiorite in Yukon: Evidence of Arc-Continent Collision: Geological Survey of Canada Paper 79–14, 27 p., doi:10.4095/105928.
Tochilin, C.J., Gehrels, G.E., Nelson, J.A., and Mahoney, B.M., 2014, U-Pb and Hf isotope analysis of detrital zircons in quartzites of the Banks Island assemblage to identify potential source terranes and origins: Lithosphere, v. 6, no. 3, p. 200–215, doi:10.1130/L338.1.
Vervoort, J.D., and Patchett, P.J., 1996, Behavior of hafnium and neodymium isotopes in the crust: Constraints from crustally derived granites: Geochimica et Cosmochimica Acta, v. 60, no. 19, p. 3717–3733, doi:10.1016/0016-7037(96)00201-3.
Vervoort, J.D., Patchett, P.J., Blichert-Toft, J., and Albarede, F., 1999, Relationships between Lu-Hf and Sm-Nd isotopic systems in the global sedimentary system: Earth and Planetary Science Letters, v. 168, p. 79–99, doi:10.1016/S0012-821X(99)00047-3.
Wheeler, J.O., and McFeely, P., 1991, Tectonic Assemblage Map of the Canadian Cordillera and Adjacent Parts of the United States of America: Geological Survey of Canada Map 1712A, scale 1:2,000,000.
White, C., Gehrels, G., Pecha, M., Giesler, D., Yokelson, I., McClelland, W., and Butler, R., 2016, U-Pb and Hf isotope analysis of detrital zircons from Paleozoic strata of the southern Alexander terrane (southeast Alaska): Lithosphere, v. 8, p. 83–96, doi:10.1130/L475.1.
Yokelson, I., Gehrels, G., Pecha, M., Giesler, D., White, C., and McClelland, W., 2015, U-Pb and Hf isotope analysis of detrital zircons from Mesozoic strata of the Gravina belt, southeast Alaska: Tectonics, v. 34, no. 10, p. 2052–2066, doi:10.1002/2015TC003955.